Solving a singular limit problem arising with Euler-Korteweg dispersive waves

Quentin Didierlaurent, Nicolas Favrie, Bruno Lombard

Solving a singular limit problem arising with Euler-Korteweg dispersive waves

Quentin Didierlaurent[a,b], Nicolas Favrie[a,c], Bruno Lombard[b,*]

[a] *Aix Marseille Univ, CNRS, IUSTI UMR 7343, Marseille, France*
[b] *Aix Marseille Univ, CNRS, Centrale Marseille, LMA UMR 7031, Marseille, France*
[c] *Department of Mathematics, Texas A&M university, College Station, Texas, USA*

Abstract

Phase transition in compressible flows involves capillarity effects, described by the Euler-Korteweg equations with non-convex equation of state. Far from phase transition, i.e. in the two convex parts of the equation of state, the dispersion terms vanish and one should recover the hyperbolic Euler equations of fluid dynamics. However, the solution of Euler-Korteweg equations does not converge towards the solution of Euler equations when dispersion tends towards zero while being non-null: it is a singular limit problem. To avoid this issue in the case of convex equation of state, a Navier-Stokes-Korteweg model is considered, whose viscosity is chosen to counterbalance exactly the dispersive terms. In the limit of small viscosity and small dispersion, the Euler model is recovered. Numerically, an extended Lagrangian method is used to integrate the Navier-Stokes-Korteweg equations so-obtained. Doing so allows to use classical numerical schemes of Godunov type with source term. Numerical results for a Riemann problem illustrate the convergence properties with vanishing dispersion.

Keywords: nonlinear dispersive waves, Euler-Korteweg equations, capillary effects, extended Lagrangian method, hyperbolic systems

1. Introduction

Numerical simulation of the dynamics of liquid-vapor phase transition, near the critical point, is of major interest in many applications: transport of cryogenic fluids in turbo pumps, polymer solvent-mixture, expansion during pipe breaks under pressure for CO2, etc.

Near the critical point, capillary forces cannot be neglected. In lines with Korteweg theory and the kinetic theory [1, 2, 3, 4], an interfacial energy is added to the total energy of the Euler model. This additional term depends on the density gradient ρ_x and on a capillarity coefficient $\mathcal{K}(\rho)$. Away from the phase transition, this interfacial energy vanishes. However,

*Corresponding author. Tel.: +33 491 84 52 42 53.
Email addresses: quentin.didierlaurent@etu.univ-amu.fr (Quentin Didierlaurent), nicolas.favrie@univ-amu.fr, nicolas.favrie@tamu.edu (Nicolas Favrie), lombard@lma.cnrs-mrs.fr (Bruno Lombard)

the solution of Euler-Korteweg equations does not converge towards the solution of the Euler equations when dispersion tends towards zero (but is non null). Such a singular limit problem is usual with nonlinear dispersive waves, and is induced by the high-order spatial derivatives involved by dispersion [5, 6]. This issue can be highlighted in the case of a Riemann problem with very small dispersion: the intermediate state differs from the one of the Euler equations, and shock's properties are modified. The main objective of this article is to fix this issue for convex equation of states. This work can be seen as a first step in solving phase transition since one want the fluid to follow Euler equations in the convex part and want the fluid to follow Euler-Korteweg equations in the non-convex part.

For this purpose, the proposed strategy is to introduce optimally an artificial viscosity $\mu(\rho)$ in the low-dispersion regime. This form of dissipative regularisation was already introduced for the Korteweg-De Vries equation [7, 8, 9], in plasma theory [10, 11] and in Lagrangian isothermal phase transition [12]. The viscosity of this Navier-Stokes-Korteweg model is chosen to counterbalance exactly the dispersion effects. This choice is driven by a linear dispersion analysis and by the study of travelling waves. In the limit of small dispersion and small viscosity, the solution of Euler model is recovered [13].

However, the mixed hyperbolic-elliptic structure of a Navier-Stokes-Korteweg model raises new numerical difficulties [14]. To overcome them, an extended Lagrangian method is used [15, 16, 17, 18, 19]. In brief, the Lagrangian of Euler-Korteweg model is modified by a penalisation term (through a parameter λ), and by an inertia term (through a parameter β). Governing equations are then derived using Hamilton's principle [20]. Finally, the viscous term is added as a source term. In this formulation, no high-order terms are introduced, so that the solution of the extended model recovers formally the solution of the original model when $(\lambda, \beta) \to (+\infty, 0)$.

The sketch of the article is then as follows. Section 2 illustrates the singular limit problem identified in [21]. Differences between the structure of the dispersive and hyperbolic waves are established. Section 3 deals with the influence of the viscosity on the dispersion analysis and on the travelling wave. The choice of the viscosity is motivated and argumented. Section 4 presents the extended Lagrangian formulation of Navier-Stokes-Korteweg model. Dispersion analysis of the extended model is given. In Section 5, the numerical strategy is shortly presented, based on splitting and on a second-order finite-volume scheme for hyperbolic systems. Numerical examples of Riemann problems show the evolution of the solution with the viscosity. When the optimal viscosity is chosen, convergence towards the solution of Euler equations is observed with vanishing viscosity.

2. Singular limit problem for vanishing dispersion

2.1. Euler-Korteweg model

We consider the 1D Euler-Korteweg (EK) model of capillary fluid. In this model, the total energy depends on the density and on the gradient of the density. The volumic Lagrangian

writes:

$$\mathcal{L} = \frac{1}{2}\rho u^2 - \rho\, e_h(\rho) - \mathcal{K}(\rho)\frac{(\varepsilon\rho_x)^2}{2},$$

where $u^2/2$ is the specific kinetic energy, $e_h(\rho)$ is the specific hydrodynamic energy, $\mathcal{K}(\rho)$ is the capillarity coefficient [22], and ε is a parameter controlling the amplitude of dispersion. Hamilton's principle of stationary action yields the EK system:

$$\text{EK}: \begin{cases} \rho_t + (\rho u)_x = 0, & \text{(1a)} \\ (\rho u)_t + \left(\rho u^2 + \rho^2 e_h' - \varepsilon^2\left[(\rho\,\mathcal{K}' - \mathcal{K})\dfrac{{\rho_x}^2}{2} + \rho\,\mathcal{K}\,\rho_{xx}\right]\right)_x = 0. & \text{(1b)} \end{cases}$$

Depending on ε, e_h, and $\mathcal{K}$, the EK system recovers various known systems (Table 1). When $\varepsilon = 0$, one obtains non-dispersive systems, notably the Euler equations of compressible flows with a convex hydrodynamic energy e_h: the relation between the thermodynamic pressure $\rho^2 {e_h}'(\rho)$ and the specific volume $1/\rho$ is a convex function. Particular values of e_h and γ lead to the system S_0 of shallow water equations.

dispersion	e_h	$\mathcal{K}$	Name	Abbreviation
0	$\rho^{\gamma-1}/(2(\gamma-1))$		Euler equations	
0	$\rho/2$		Shallow water ($\gamma = 2$)	S_0
ε	$\rho/2$	$1/(4\rho)$	Defocusing Nonlinear Schrödinger	S_ε

Table 1: Various forms of the Euler-Korteweg system. $\gamma > 1$ is the polytropic coefficient.

When $\varepsilon \neq 0$, dispersive systems are obtained, which are not hyperbolic in the sense of Lax [23]. A particular form of $\mathcal{K}$ leads to the hydrodynamic form of the defocusing nonlinear Schrödinger equation [24, 16, 25], denoted by S_ε. This system is integrable, with known exact solutions.

2.2. Illustration of the singular limit problem

The objective of this part is to highlight a singular limit problem of the system S_ε when $\varepsilon \to 0$. The two systems studied here are:

$$S_0: \begin{cases} \rho_t + (\rho u)_x = 0, & \text{(2a)} \\ (\rho u)_t + \left(\rho u^2 + \dfrac{\rho^2}{2}\right)_x = 0, & \text{(2b)} \end{cases}$$

and

$$S_\varepsilon: \begin{cases} \rho_t + (\rho u)_x = 0, & \text{(3a)} \\ (\rho u)_t + \left(\rho u^2 + \dfrac{\rho^2}{2} - \dfrac{\varepsilon^2\rho}{4}\left(\dfrac{\rho_x}{\rho}\right)_x\right)_x = 0. & \text{(3b)} \end{cases}$$

A Riemann problem (RP) is considered, with x_c the position of the initial discontinuity and $\rho_L > \rho_R$:

$$u(x,0) = 0, \quad \rho(x,0) = \begin{cases} \rho_L, & x < x_c, \\ \rho_R, & x > x_c. \end{cases} \tag{4}$$

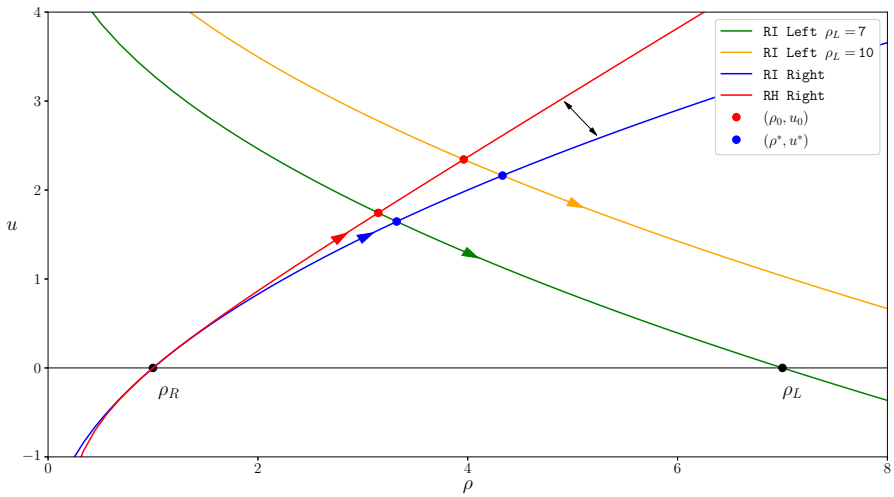

Figure 1: RI curves and RH curve in the (ρ, u) plane. Intersections between the curves give the plateau values. The black arrow shows the increasing gap between (ρ^*, u^*) and (ρ_0, u_0) when ρ_L increases.

Solution of system S_0. The complete derivation of the analytical solution can be found in many reference books [26, 27]. Here we only give the main results for completeness. For $t > 0$, the initial discontinuity splits into a right-going shock wave (SW), a left-going centered rarefaction wave and an intermediate plateau (ρ_0, u_0). The shock intensity and the shock speed are determined by the Rankine-Hugoniot jump conditions:

$$[\![\rho]\!]\, D = [\![\rho u]\!]\,, \tag{5}$$

$$[\![\rho u]\!]\, D = \left[\!\!\left[\rho u^2 + \frac{\rho^2}{2}\right]\!\!\right], \tag{6}$$

where D is the shock speed and $[\![f]\!] = f_R - f$ is the jump of a given f across the SW. Eliminating D in (6) by using (5) gives the "Right Rankine-Hugoniot Locus" (RH Right) in the (ρ, u) plane:

$$u = (\rho - \rho_R)\sqrt{\frac{1}{2}\left(\frac{1}{\rho} + \frac{1}{\rho_R}\right)}. \tag{7}$$

In a left-going rarefaction wave, the Riemann invariant $r = u + 2\sqrt{\rho}$ is conserved. This equation gives the "Left Riemann invariant Locus" (RI Left) in the (ρ, u) plane:

$$u = 2\left(\sqrt{\rho_L} - \sqrt{\rho}\right). \tag{8}$$

Intersection of (7) and (8) gives the plateau value (ρ_0, u_0):

$$2(\sqrt{\rho_L} - \sqrt{\rho_0}) - (\rho_0 - \rho_R)\sqrt{\frac{1}{2}\left(\frac{1}{\rho_0} + \frac{1}{\rho_R}\right)} = 0, \tag{9}$$

$$u_0 = 2(\sqrt{\rho_L} - \sqrt{\rho_0}), \tag{10}$$

represented in Figure 1 for various values of ρ_L and ρ_R.

Solution of system S_ε. The RP problem for S_ε is better known as a "Gurevich-Pitaevskii problem" [28]. The exact solution has been constructed in [25]. The asymptotic solution in time is composed of a left-going centered rarefaction wave (same as system S_0), a right-going dispersive shock wave (DSW) and a plateau (ρ^*, u^*). The DSW is a wave train modulated in amplitude and wavenumber. Modulation theory gives its analytical expression and its Whitham envelope [29, 25, 16]. The plateau is given by the intersection of a "RI Left" and a "RI Right" curve:

$$u = 2\left(\sqrt{\rho_L} - \sqrt{\rho}\right), \quad u = 2\left(\sqrt{\rho} - \sqrt{\rho_R}\right), \tag{11}$$

leading to:

$$u^* = \sqrt{\rho_L} - \sqrt{\rho_R}, \tag{12}$$

$$\rho^* = \frac{1}{4}\left(\sqrt{\rho_L} + \sqrt{\rho_R}\right)^2. \tag{13}$$

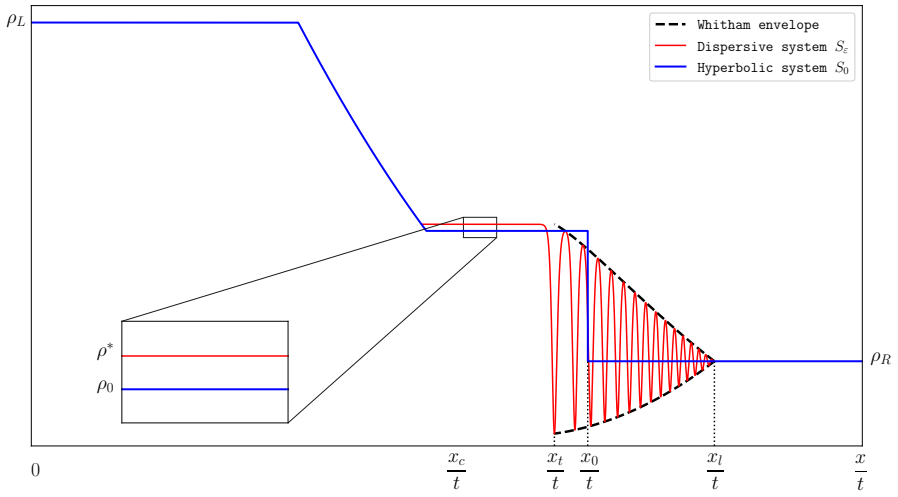

Figure 2: Exact solution of S_0 and asymptotic solution of S_ε in x/t. The parameters are $\rho_L = 5$, $\rho_R = 1$. Particular points are: x_t the position of the trailing edge, x_l the position of the leading edge, and x_0 the position of the shock wave.

Comparison between both solutions. The solutions of S_0 and S_ε are compared in Figure 2. Three main differences are observed. Firstly, the SW is a discontinuity at x_0, whereas the DSW has a finite length $x_t - x_l$. This length increases with time and is independent of ε [25]:

$$x_t - x_l = \left(\sqrt{\rho^*} - \frac{8\rho^* - 8\sqrt{\rho^* \rho_R} + \rho_R}{2\sqrt{\rho^*} - \sqrt{\rho_R}} \right) t.$$

The only influence of ε is on the wavelength $\ell = (2\pi)/k$ of oscillations in the DSW, with

$$k(m, \varepsilon) = \frac{2\pi}{J(m)} \frac{\sqrt{\rho_1 - \rho_3}}{\varepsilon}, \quad m = \frac{\rho_2 - \rho_3}{\rho_1 - \rho_3},$$

where m is the modulation parameter, $\rho_1 > \rho_2 > \rho_3$the modulated amplitudes, and $J(m)$ the elliptic integral of the first kind [25]. Secondly, the difference of plateau (ρ_0, u_0) and plateau (ρ^*, u^*) comes from the difference between (9) and (13), and it is highlighted in Figure 1. When $\rho_L - \rho_R$ is large, the gap between (ρ_0, u_0) (red dot) and (ρ^*, u^*) (blue dot) increases, as highlighted by the black arrow in Figure 1. Moreover, (9) and (13) do not depend on ε. Therefore:

$$\lim_{\varepsilon \to 0} \rho^* \neq \rho_0, \quad \lim_{\varepsilon \to 0} u^* \neq u_0.$$

To summarize this section, the solutions of S_0 and S_ε have different structures, induced by the difference between SW and DSW. The solutions are self-similar with respect to the change of variable $(x, t) \to (x/\varepsilon, t/\varepsilon)$. Consequently, the differences between the solutions never vanish when $\varepsilon \to 0$.

3. Strategy to fix the singular limit problem

3.1. Navier-Stokes-Korteweg model

To by-pass this singular limit problem, introduction of an optimal viscosity $\tau\mu$ is considered. The parameter τ controls the effect of viscosity and will be compared to the dispersive parameter ε. EK system (1) becomes the Navier-Stokes-Korteweg (NSK) system:

$$\text{NSK}: \begin{cases} \rho_t + (\rho u)_x = 0, & \text{(14a)} \\ (\rho u)_t + \left(\rho u^2 + \rho^2 e_h{}' - \varepsilon^2 \left[(\rho \mathcal{K}' - \mathcal{K}) \frac{{\rho_x}^2}{2} + \rho \mathcal{K} \rho_{xx} \right] - \tau\mu\, u_x \right)_x = 0. & \text{(14b)} \end{cases}$$

The idea is to find the functions $\tau := \hat{\tau}$ and $\mu := \hat{\mu}$ which cancel the dispersion introduced by $\mathcal{K}$ and ε. Those functions are obtained in two ways: performing the dispersion analysis, and exhibiting a travelling wave solution. It will be the subject of the two next subsections.

3.2. Dispersion analysis

Here, we prove by a dispersion analysis that a particular choice of $\hat{\tau}\hat{\mu}$ can lead to dispersive-less properties: wave's speed of propagation can be rendered independent of the wavenumber κ

whatever ε. Galilean invariance of NSK system (14) allows to choose a uniform state $(\overline{\rho}, \bar{u} = 0)$. Linearization of the NSK around this uniform states leads to:

$$\begin{cases} \tilde{\rho}_t + \overline{\rho}\tilde{u}_x = 0, & \text{(15a)} \\ \overline{\rho}\tilde{u}_t + \overline{c^2}\tilde{\rho}_x - \varepsilon^2\overline{\rho}\,\mathcal{K}(\overline{\rho})\tilde{\rho}_{xxx} - \tau\mu(\overline{\rho})\tilde{u}_{xx} = 0, & \text{(15b)} \end{cases}$$

where $(\tilde{\rho}, \tilde{u})$ are fluctuations around the uniform state, and $\overline{c} = \sqrt{(\overline{\rho^2 e'})'}$ is the sound speed of the uniform state. Assuming harmonic solution of the form $\exp(\mathrm{i}(\omega t - \kappa x))$, where ω is the angular frequency, the phase velocity $c_p = \omega/\kappa$ is:

$$c_p(\kappa) = \mathrm{i}\,\tau\kappa\,\frac{\mu(\overline{\rho})}{2\overline{\rho}} \pm \sqrt{\overline{c}^2 + \kappa^2\left(\varepsilon^2\overline{\rho}\,\mathcal{K}(\overline{\rho}) - \tau^2\frac{\mu(\overline{\rho})^2}{4\overline{\rho^2}}\right)}. \tag{16}$$

The real part of (16) depends on κ, which is the signature of a dispersive wave. If we choose

$$\tau := \hat{\tau} = \varepsilon, \tag{17}$$

$$\mu := \hat{\mu} = 2\,\overline{\rho}\sqrt{\overline{\rho}\,\mathcal{K}(\overline{\rho})}, \tag{18}$$

then (16) degenerates into

$$\hat{c}_p(\kappa) = \mathrm{i}\,\varepsilon\kappa\sqrt{\overline{\rho}\,\mathcal{K}(\overline{\rho})} \pm \overline{c}. \tag{19}$$

The real part of the phase velocity no longer depends on κ, and thus dispersion is canceled. In line with the "viscosity method" [30, 31, 32], the solutions of NSK tend towards the solutions of the Euler equations when viscosity vanishes: no singular limit problem occurs. It leads to conjecture that the solution of NSK tends towards the solution of the Euler equations when $\varepsilon \to 0$. Numerical simulations will confirm this hypothesis.

3.3. Travelling wave

In this section, $\tau := \hat{\tau} = \varepsilon$ and μ is arbitrary. Using the change of variables $(x, t) \to \xi = (x - D\,t)/\varepsilon$, (14a) becomes:

$$q = \rho\,(u - D), \tag{20}$$

where q is the constant flow rate of fluid across the wave and is chosen to be negative. Integration of (14b) and use of (20) gives

$$\frac{q^2}{\rho} + \rho^2 e_h{}'(\rho) + \mu(\rho)\frac{q}{\rho^2}\left(\frac{d\rho}{d\xi}\right) - \rho^2\left[\left(\frac{\mathcal{K}}{\rho}\right)'\frac{1}{2}\left(\frac{d\rho}{d\xi}\right)^2 + \frac{\mathcal{K}}{\rho}\left(\frac{d^2\rho}{d\xi^2}\right)\right] = C_1, \tag{21}$$

where C_1 describes the constant right-state R at infinity:

$$C_1 = \frac{q^2}{\rho_R} + {\rho_R}^2 e_h{}'(\rho_R).$$

After multiplying (21) by $-\frac{1}{\rho^2}\frac{d\rho}{d\xi}$, one integration yields a Lyapunov function E (see Appendix A)

$$E\left(\rho, \frac{d\rho}{d\xi}\right) = \frac{1}{2}\frac{\mathcal{K}(\rho)}{\rho}\left(\frac{d\rho}{d\xi}\right)^2 - e_h(\rho) - \frac{C_1}{\rho} + \frac{q^2}{2\rho^2},$$

which, according to (21), decreases along trajectories of the system in the phase space:

$$\frac{dE}{d\xi} = q\,\frac{\mu(\rho)}{\rho^4}\left(\frac{d\rho}{d\xi}\right)^2 < 0. \tag{22}$$

The local extrema ρ_c of E verify the following conditions:

$$\left.\frac{d\rho}{d\xi}\right|_{\rho_c} = 0, \quad \frac{q^2}{\rho_R} + {\rho_R}^2 {e_h}'(\rho_R) = {\rho_c}^2 {e_h}'(\rho_c) + \frac{q^2}{\rho_c}. \tag{23}$$

Additional details about the extrema are given in Appendix B. Setting $c = \sqrt{(\rho^2\, {e_h}')'}$ the sound speed and $M = (u - D)/c$ the Mach number, the linearized version of (21) around the extrema is:

$$\frac{d^2\Delta\rho}{d\xi^2} - 2\theta\frac{c_c M_c}{\sqrt{\rho_c \mathcal{K}_c}}\frac{d\Delta\rho}{d\xi} + \frac{{c_c}^2({M_c}^2 - 1)}{\rho_c \mathcal{K}_c}\Delta\rho = 0, \quad \theta = \frac{\mu_c}{2\rho_c\sqrt{\rho_c \mathcal{K}_c}}, \tag{24}$$

where $\Delta\rho = \rho - \rho_c$. The analysis is reduced to the study of a damped harmonic oscillator with θ the damping ratio. Eigenwavenumbers are:

$$k_c = \frac{c_c M_c}{\sqrt{\rho_c \mathcal{K}_c}}\left[\theta \pm \sqrt{(\theta^2 - 1) + \frac{1}{{M_c}^2}}\right]. \tag{25}$$

Non-oscillating solutions of (24) correspond to real-valued eigenwavenumber. Assuming that c_c is a real-valued function, we have to choose $\theta \geq 1$. This condition is also known as the *tame capillarity* condition [13]. The choice $\theta^2 = 1 - 1/{M_c}^2$ is not adequate since θ is complex-valued in region where ${M_c}^2 < 1$.

Numerical simulations of the ODE (21) is considered. Initial conditions are:

$$\text{IC} \;:\; \begin{cases} \rho(0) = \rho_0 - 10^{-5}, & \text{(26a)} \\ \left.\dfrac{d\rho}{d\xi}\right|_{\xi=0} = 0. & \text{(26b)} \end{cases}$$

Figure 3 illustrates various regimes obtained for different values of θ. The red dot corresponds to the state ρ_0 and the purple dot to the state ρ_R. The numerical simulations are obtained by the RK4 method. Numerical results in Figure 3-(b,c) confirm our choice for θ. Comparing the solution with $\varepsilon = 0.5$ show that the thickness of the wave is large when θ is large ($\theta \gg 1$). As a consequence, $\theta = 1$ will be the choice in forthcoming numerical simulations.

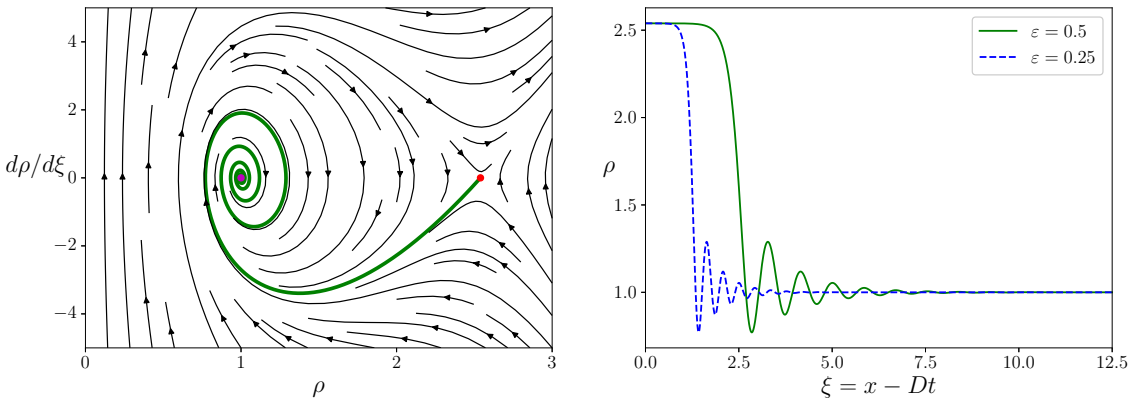

(a) Pseudo-periodic regime ($\theta = 0.1 < 1$)

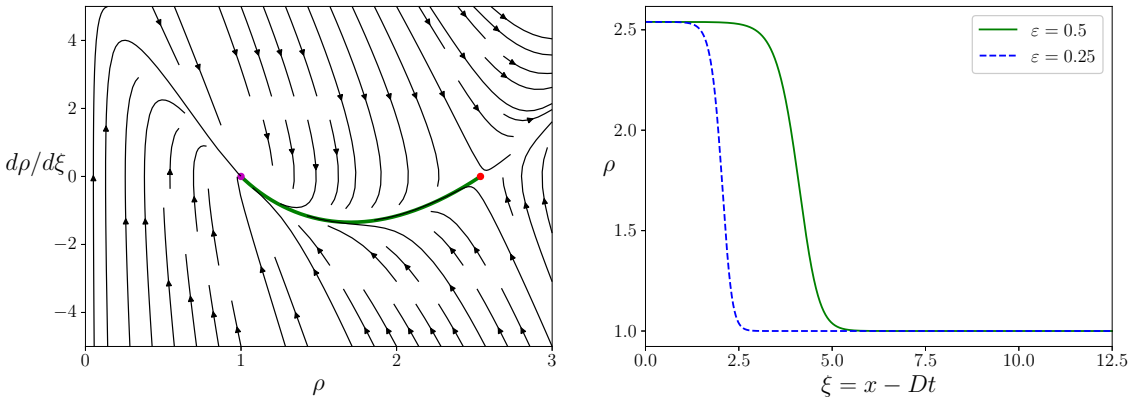

(b) Critical regime ($\theta = 1$)

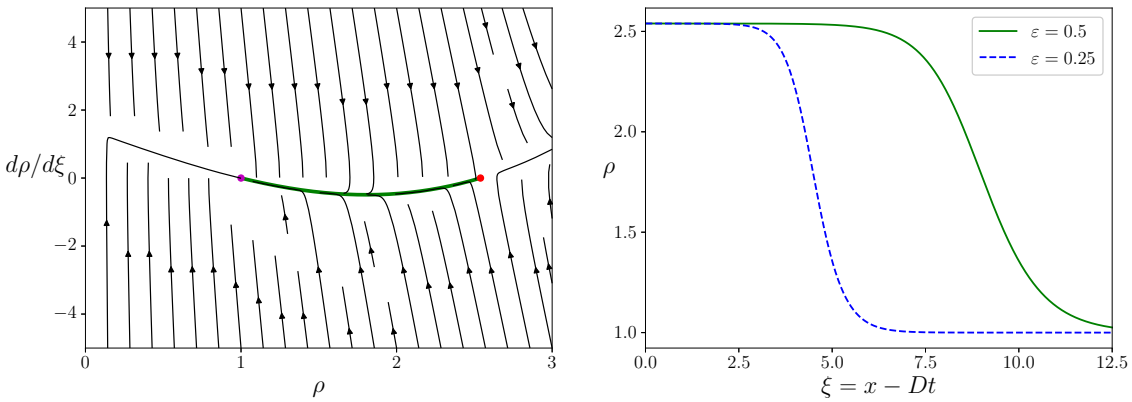

(c) Overdamped regime ($\theta = 3$)

Figure 3: Left: the phase portrait and one solution for $\varepsilon = 0.5$. Right: density for various ε.

4. Extended Lagrangian formulation

4.1. Principle

Numerical schemes for NSK-type systems are not classical due to the "mixed hyperbolic-elliptic" structure of the system [14]. One way is to solve a discrete elliptic/parabolic operator on the whole computational domain and to solve the hyperbolic part locally. An example of such scheme is given in [33] for the Serre-Green-Naghdi model. This method provides good results but at a high computational cost. To overcome this issue, an extended Lagrangian formulation was proposed in [15]. The original system, named the *master system*, is replaced by an approximate hyperbolic system, named the *extended system*, composed of a new variable η close to ρ. The extended solution recovers the behavior of the master solution in some limit.

This formulation was successfully applied to a wide list of nonlinear wave phenomena, to cite a few: DNS equation in quantum mechanics [16], thin films down an inclined plane [17], Ericksen bar model in solid mechanics [18], and BBM equations [19]. The detailed description of this formulation can be found in the aforementioned articles and is shortly presented in the next subsection.

4.2. Extended Euler-Korteweg model

We recall the master Lagrangian of the EK system (1)

$$\mathcal{L} = \frac{1}{2}\rho\, u^2 - \left(\rho\, e_h(\rho) + \mathcal{K}(\rho)\frac{(\varepsilon\rho_x)^2}{2}\right).$$

This Lagrangian is extended by adding new terms:

- a penalisation term: $\lambda\,\dfrac{\rho}{2}\left(\dfrac{\eta}{\rho}-1\right)^2$, where η is a new variable;
- a kinetic energy term: $\dfrac{1}{2}\,\rho\,\beta\left(\dfrac{d\eta}{dt}\right)^2$, analogous to a term involved in bubbly flows [20].

The parameter λ (resp. β) controls the penalisation (resp. the inertia) term. Replacing ρ_x by η_x and setting new variables $p=\eta_x$ and $w=d\eta/dt$, the extended Lagrangian $\mathcal{L}_e$ writes:

$$\mathcal{L}_e = \frac{1}{2}\rho\,\beta\, w^2 + \frac{1}{2}\rho\, u^2 - \left(\rho\, e_h(\rho) + \mathcal{K}(\rho)\frac{(\varepsilon p)^2}{2} + \lambda\,\frac{\rho}{2}\left(\frac{\eta}{\rho}-1\right)^2\right).$$

By applying twice a variational principle (see the methodology in the appendix of [16]) and adding evolution equations for η,w and p, we obtain the extended EK system:

$$\mathrm{EK}_e : \begin{cases} \rho_t + (\rho u)_x = 0, & \text{(27a)}\\ (\rho u)_t + \left(\rho u^2 + \rho^2\, e' + \varepsilon^2\dfrac{p^2}{2}\,(\rho\,\mathcal{K}' + \mathcal{K}) + \lambda\eta\left(1-\dfrac{\eta}{\rho}\right)\right)_x = 0, & \text{(27b)}\\ (\rho\eta)_t + (\rho u\eta)_x = \rho w, & \text{(27c)}\\ (\rho w)_t + \left(\rho u w - \varepsilon^2\dfrac{\mathcal{K}p}{\beta}\right)_x = \dfrac{\lambda}{\beta}\left(1-\dfrac{\eta}{\rho}\right), & \text{(27d)}\\ p_t + (pu - w)_x = 0. & \text{(27e)} \end{cases}$$

We expect that $\eta = \rho + \mathcal{O}(1/\lambda) + \mathcal{O}(\beta)$, so that the extended EK system recovers the master system (1) when $\lambda \to +\infty$ and $\beta \to 0$. This property has been justified rigorously in [34] in the case of Serre-Green-Naghdi model with $\beta = 1$, and we suppose it to be valid here. Injecting (27d) into (27b) leads to:

$$(\rho u)_t + \left(\rho u^2 + \rho^2 e' + \beta \rho \eta \frac{dw}{dt} - \varepsilon^2 \left[((2\eta - \rho)\mathcal{K}' - \mathcal{K}) \frac{p^2}{2} + \eta \mathcal{K} p_x \right] \right)_x = 0,$$

where $dw/dt = w_t + u w_x$. When $(\lambda, \beta) \to (\infty, 0)$, and assuming that $\eta \to \rho$ and $p \to \rho_x$, then one recovers (14b) of the EK system.

4.3. Extended Navier-Stokes-Korteweg model

As proposed in [18], the viscosity is introduced as an additional source term in (27d). This leads to:

$$\mathrm{NSK}_e : \begin{cases} \rho_t + (\rho u)_x = 0, & \text{(28a)} \\ (\rho u)_t + \left(\rho u^2 + \rho^2 e' + \varepsilon^2 \dfrac{p^2}{2} (\rho \mathcal{K}' + \mathcal{K}) + \lambda \eta \left(1 - \dfrac{\eta}{\rho} \right) \right)_x = 0, & \text{(28b)} \\ (\rho \eta)_t + (\rho u \eta)_x = \rho w, & \text{(28c)} \\ (\rho w)_t + \left(\rho u w - \varepsilon^2 \dfrac{\mathcal{K} p}{\beta} \right)_x = \dfrac{\lambda}{\beta} \left(1 - \dfrac{\eta}{\rho} \right) - \tau \dfrac{\mu(\rho)}{\beta \rho^2} w, & \text{(28d)} \\ p_t + (pu - w)_x = 0. & \text{(28e)} \end{cases}$$

Injecting (28d) into (28b) and using (28a), we recover NSK model when $\lambda \to \infty$ and $\beta \to 0$.

4.4. Characteristic speeds

NSK_e system (28) can be put in a quasi-linear form:

$$\mathbf{W}_t + \mathbf{A}(\mathbf{W}) \mathbf{W}_x = \mathbf{B}(\mathbf{W}), \tag{29}$$

where $\mathbf{A}(\mathbf{W})$ is a 5×5 matrix given in Appendix C and $\mathbf{W} = (\rho, u, \eta, w, p)^\top$ is the vector of primitive (non-conservative) variable and $\mathbf{B}(\mathbf{W})$ a vector that contains the source term. The five eigenvalues/characteristic speeds α_i of the system are given in Appendix C. In general, the hyperbolicity for such a general case is not proven. If we consider the case of the extended DNS system (Table 1), hyperbolicity has been proved in [16] when $\lambda \geq 0$ and $\beta > 0$. The five eigenvalues are then:

$$\alpha^1 = u, \quad \alpha^{2,3} = u \pm \sqrt{\rho + \lambda \frac{\eta^2}{\rho^2}}, \quad \alpha^{4,5} = u \pm \sqrt{\frac{\varepsilon^2}{4 \beta \rho^2}}. \tag{30}$$

These eigenvalues will be useful for the numerical method detailed in Section 5.1.

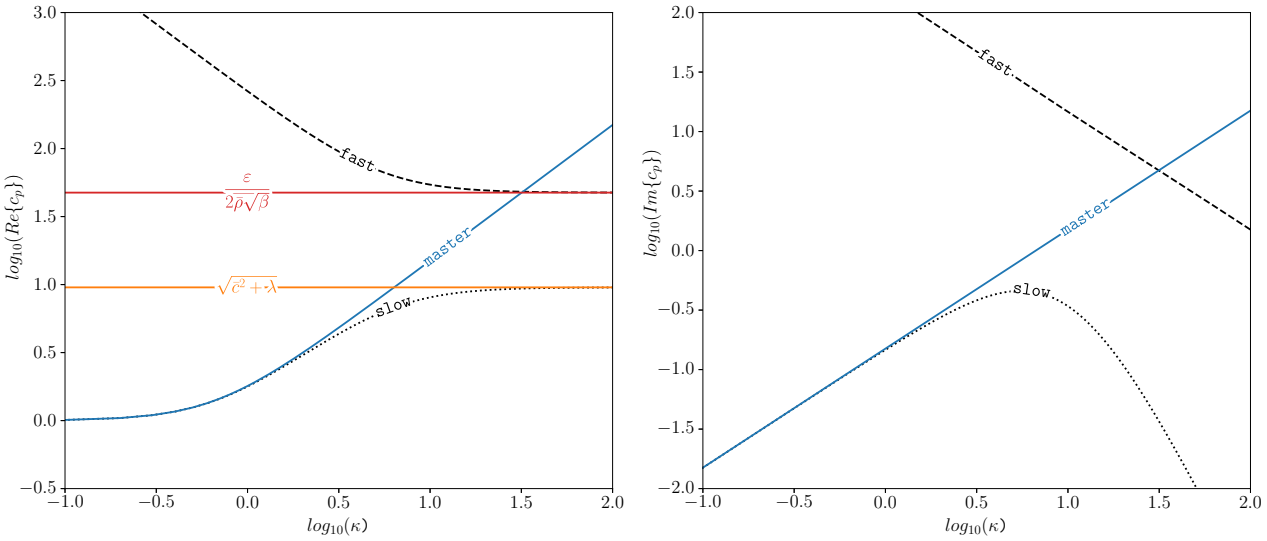

(a) (b)

Figure 4: Dispersion curve of the linearized NSK_e system, with $\lambda = 200$, $\beta = 0.003$, $\bar{\mu} = 0.1$, $\varepsilon = \tau = 3$, $\bar{\rho} = 1$.

4.5. Choice of (λ, β)

When using the extended Lagrangian method, it is important to estimate the error of this formulation. To do so, a dispersion analysis of the linearized extended system is usually carried out [15, 16, 18, 17, 19]. We provide a similar analysis here for the NSK_e system in the case of DNS ($e_h(\rho) = \rho/2$ and $\mathcal{K}(\rho) = 1/(4\rho)$). Using the same notation as in Section 3.2 and assuming that the phase velocity $c_p \neq 0$, we obtain a quartic expression:

$$(c_p)^4 + (c_p)^3 \frac{\mathrm{i}\bar{\mu}\tau}{\beta\bar{\rho}^3\kappa} - (c_p)^2 \left(\frac{\lambda}{\beta\bar{\rho}^2\kappa^2} + \lambda + \bar{c}^2 + \frac{\varepsilon^2}{4\beta\bar{\rho}^2} \right) - (c_p) \frac{\mathrm{i}\bar{\mu}\tau(\lambda + \bar{c}^2)}{\beta\bar{\rho}^3\kappa} + (\lambda + \bar{c}^2) \frac{\varepsilon^2}{4\beta\bar{\rho}^2} + \frac{\lambda\bar{c}^2}{\beta\bar{\rho}^2\kappa^2} = 0,$$

where the uniform state is $(\bar{\rho}, \bar{u} = 0, \bar{\eta} = \bar{\rho}, \bar{p} = 0, \bar{w} = 0)$. Assuming a positive phase velocity, this equation have two solutions namely the *slow wave* ${c_p}^-$ and the *fast wave* ${c_p}^+$. Comparison with the phase speed of the *master wave* (Section 3.2) is given in Figure 4. The slow wave is related to the master wave since it shares the same limit when $\kappa \to 0$. The fast wave is a spurious wave induced by the modification of the Lagrangian. The limits of the slow wave and of the fast wave when $\kappa \to \infty$ are:

$$\lim_{k \to +\infty} \Re\{{c_p}^{(+)}\} = \max\left(\sqrt{\bar{\rho} + \lambda}, \sqrt{\frac{\varepsilon^2}{4\,\beta\,\bar{\rho}^2}} \right), \quad \lim_{k \to +\infty} \Re\{{c_p}^{(-)}\} = \min\left(\sqrt{\bar{\rho} + \lambda}, \sqrt{\frac{\varepsilon^2}{4\,\beta\,\bar{\rho}^2}} \right). \tag{31}$$

In the inviscid case ($\mu = 0$), one condition has to be fulfilled to ensure that the slow wave mimics the master wave [18]. This condition is due to the dispersive nature of the master system. In the case of DNS, the dispersion is positive [25, 21, 35]: c_p increases with κ. Therefore, the following condition has to be fulfilled by $\bar{\rho}$:

$$\min\left(\bar{\rho} + \lambda, \frac{\varepsilon^2}{4\,\beta\,\bar{\rho}^2} \right) > \bar{\rho}. \tag{32}$$

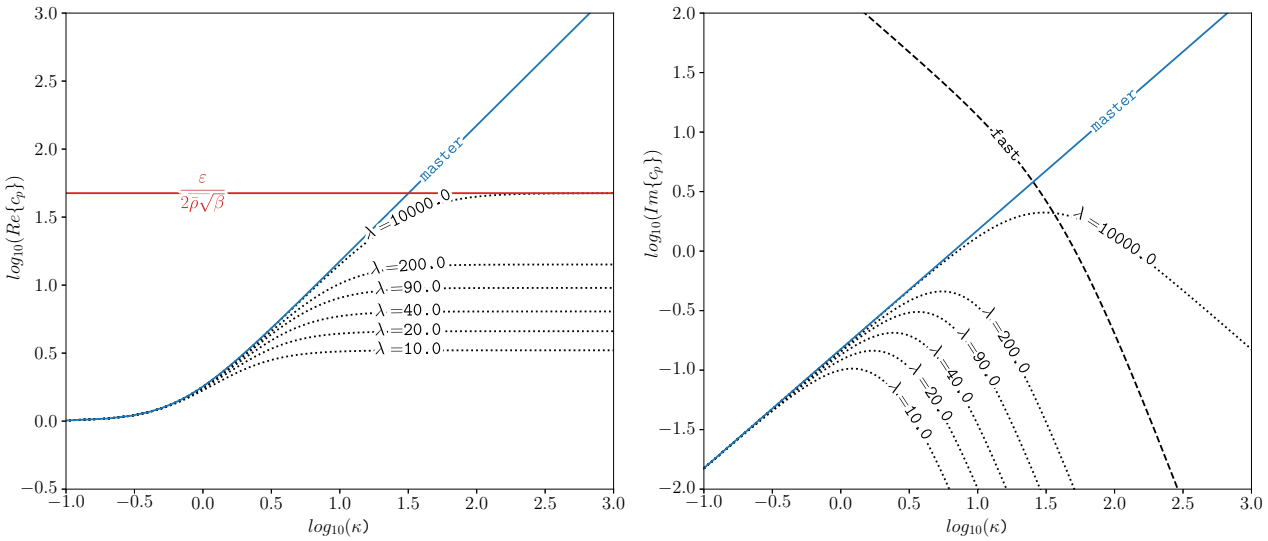

(a) (b)

Figure 5: Dispersion curve of the linearized NSK_e system for various λ. Parameters: $\beta = 0.003$, $\bar{\mu} = 0.1$, $\varepsilon = \tau = 3$, $\bar{\rho} = 1$.

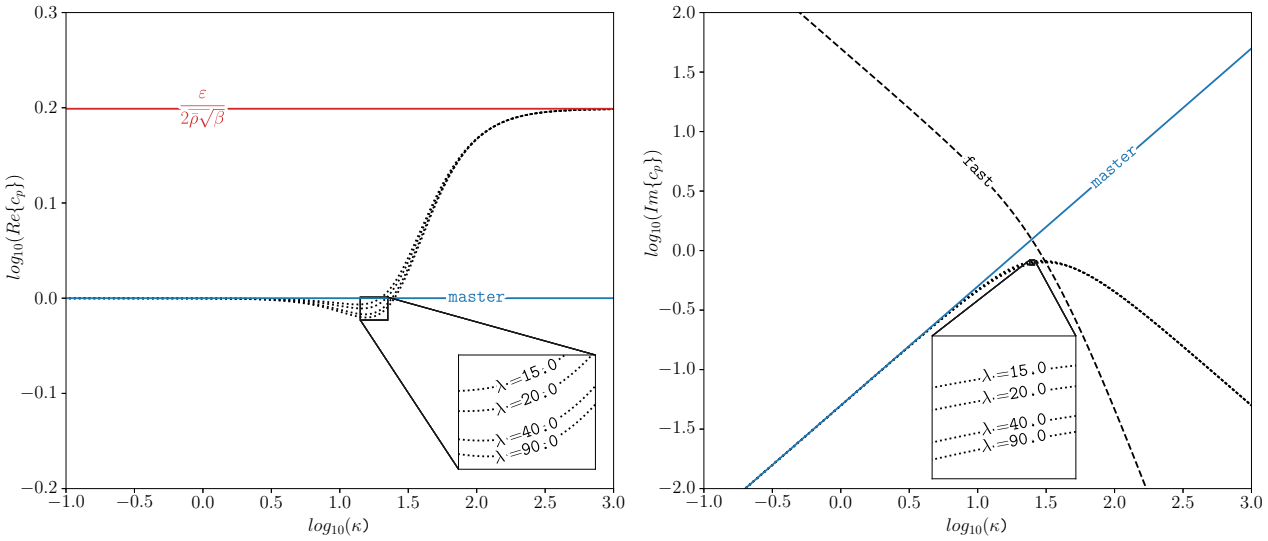

(a) (b)

Figure 6: Dispersion curve of the linearized NSK_e system for various λ when $\bar{\mu} = \hat{\mu}(\bar{\rho})$. Parameters: $\beta = 0.003$, $\varepsilon = \tau = 0.1$, $\bar{\rho} = 1$.

From (16), the dispersion is still positive when $\mu \leq \hat{\mu}$. Consequently, we suppose that the condition (32) holds in this case. Figure 5 shows the behavior of the slow wave for variable λ and a given β. As λ increases, the slow wave mimics the master wave. For a critical value of λ, the slow wave is bounded by the limit of the fast wave (see the slow wave for $\lambda = 10^4$ in Figure 5 (a), as described by (31)). To avoid this bound, β has to be decreased. The case where $\bar{\mu} = \hat{\mu}(\bar{\rho})$ is shown in Figure 6. The master wave speed is constant and equal to the local sound speed. From the zoom, it is clear that λ has no influence on the behavior of the slow wave when $\varepsilon \to 0$. The relevant parameter is then β, and it can be chosen properly. Indeed, the condition (32) becomes:

$$\frac{\varepsilon^2}{4\beta\,\bar{\rho}^2} \geq \bar{\rho} \iff \beta \leq \frac{\varepsilon^2}{4\,\bar{\rho}^3}. \tag{33}$$

To summarize, the slow wave mimics the behavior of the master wave for a limited range of wavenumbers, when $\lambda \to \infty$ and $\beta \to 0$. In the case where $\mu = \hat{\mu}(\bar{\rho})$ and $\varepsilon \to 0$, β has to satisfy (33).

5. Numerical results

5.1. Numerical methods

The NSK_e system can be recast as:

$$\mathbf{U}_t + \mathbf{F}(\mathbf{U})_x = \mathbf{S}(\mathbf{U}), \tag{34}$$

with $\mathbf{U} = (\rho, \rho u, \rho\eta, \rho w, p)^\top$ the vector of conserved quantities, $\mathbf{F}(\mathbf{U})$ a vector of physical fluxes and $\mathbf{S}(\mathbf{U})$ a vector that contains the source term. To simulate numerically (34), we apply a Godunov splitting [27, 26]:

$$\text{Step 1 : compute } \mathbf{U}^* \text{ :} \begin{cases} \text{PDE} : \mathbf{U}_t + \mathbf{F}(\mathbf{U})_x = \mathbf{0}, & \text{(35a)} \\ \text{IC} : \mathbf{U}^n. & \text{(35b)} \end{cases}$$

$$\text{Step 2 : compute } \mathbf{U}^{n+1} \text{ :} \begin{cases} \text{ODE} : \mathbf{U}_t = \mathbf{S}(\mathbf{U}), & \text{(36a)} \\ \text{IC} : \mathbf{U}^*. & \text{(36b)} \end{cases}$$

The spatial domain $[0, L]$ is discretized into N cells. The volume of each cells is $\Delta x = \frac{L}{N}$ and the central position of a cell i is set at x_i. The time step is $\Delta t = t^{n+1} - t^n$. We define by $\mathbf{U}_i^n$ the average of $\mathbf{U}$ over a cell at t^n and $\mathbf{F}_{i\pm\frac{1}{2}}$ the numerical fluxes at the boundary of a cell. At the beginning of Step 1, characteristics speed ${\alpha_i}^1$,${\alpha_i}^2$, ... ,${\alpha_i}^p$ are computed based on $\mathbf{U}_i^n$. The time step is obtained from the Courant-Friedrichs-Lewy condition:

$$\text{CFL} = \frac{\alpha_{max}\,\Delta t}{\Delta x} \leq 1, \quad \alpha_{max} = \max_{i,p}(|\alpha_i^p|),$$

where α_{max} is the maximum of all the characteristic speeds over the spatial domain. The second-order TVD MUSCL-Hancock method [27] applied on $\mathbf{U}_i^n$ gives boundary extrapolated

values $\mathbf{U}_i^{L,R}$ based on limited slopes; the MINMOD limiter is used for this purpose. Numerical fluxes $\mathbf{F}_{i+\frac{1}{2}}$ are estimated using HLL flux:

$$\mathbf{F}_{i+\frac{1}{2}} = \mathbf{F}_{\mathrm{L}} \quad \text{if } \mathrm{S}_{\mathrm{L}} > 0, \tag{37}$$

$$\mathbf{F}_{i+\frac{1}{2}} = \mathbf{F}_{\mathrm{R}} \quad \text{if } \mathrm{S}_{\mathrm{R}} < 0, \tag{38}$$

$$\mathbf{F}_{i+\frac{1}{2}} = \frac{\mathrm{S}_{\mathrm{R}}\mathbf{F}_{\mathrm{L}} - \mathrm{S}_{\mathrm{L}}\mathbf{F}_{\mathrm{R}} + \mathrm{S}_{\mathrm{L}}\mathrm{S}_{\mathrm{R}}(\mathbf{U}_{i+1}^{L} - \mathbf{U}_i^{R})}{\mathrm{S}_{\mathrm{R}} - \mathrm{S}_{\mathrm{L}}} \quad \text{else,} \tag{39}$$

with $\mathbf{F}_{\mathrm{L}} = \mathbf{F}(\mathbf{U}_i^R)$, $\mathbf{F}_{\mathrm{R}} = \mathbf{F}(\mathbf{U}_{i+1}^L)$ and S_{L}, S_{R} defined as follows:

$$\mathrm{S}_{\mathrm{L}} = \min_{p\in\{0,2,4\}}(\alpha_i{}^p, \alpha_{i+1}{}^p), \tag{40}$$

$$\mathrm{S}_{\mathrm{R}} = \max_{p\in\{0,1,3\}}(\alpha_i{}^p, \alpha_{i+1}{}^p). \tag{41}$$

The time derivative is approximated by a first-order Euler method. Averaging (35a) over a cell volume gives:

$$\mathbf{U}_i^* = \mathbf{U}_i^n + \frac{\Delta t}{\Delta x}\left(\mathbf{F}_{i-\frac{1}{2}} - \mathbf{F}_{i+\frac{1}{2}}\right).$$

Step 2 corresponds to the following system:

$$\begin{cases} \dfrac{d\rho}{dt} = 0, \quad \dfrac{d\rho u}{dt} = 0, \quad \dfrac{dp}{dt} = 0, & \text{(42a)} \\ \dfrac{d\rho\eta}{dt} = \rho w, & \text{(42b)} \\ \dfrac{d\rho w}{dt} = \dfrac{\lambda}{\beta}\left(1 - \dfrac{\eta}{\rho}\right) - \dfrac{\tau\mu(\rho)}{\beta\rho^2}w. & \text{(42c)} \end{cases}$$

From equations (42a), it follows $\rho = \rho^*$, $u = u^*$, $p = p^*$. Equations (42b) and (42c) are equivalent to the second-order ODE:

$$\frac{d^2\eta}{dt^2} + \frac{\tau\mu^*}{\beta\rho^{*3}}\frac{d\eta}{dt} + \frac{\lambda}{\beta\rho^{*2}}\eta = \frac{\lambda}{\beta\rho^*}, \tag{43}$$

where $\mu^* = \mu(\rho^*)$. This system has exact solutions given in Appendix D. From numerical experiments (see Appendix E), the following dependence in ε is observed:

$$\rho \sim \rho_1(x) + \varepsilon\, f(x), \quad u \sim u_1(x) + \varepsilon\, h(x), \quad \eta \sim \eta_1(x) + \varepsilon\, g(x), \quad w \sim w_1(x)\frac{1}{\varepsilon}, \quad p \sim p_1(x).\frac{1}{\varepsilon}$$

The functions $\rho_1, u_1, \eta_1, w_1, p_1$ correspond respectively to the fields ρ, u, η, w, p when $\varepsilon = 1$, and thus are independent of ε. Moreover, one deduces from the dispersion analysis $\tau = \varepsilon$ and $\beta \sim \varepsilon^2$. With those scaling, the eigenvalues of $\mathbf{A}$ are independent of ε and the eigenvalues of the source term (see Appendix D) scale like $1/\varepsilon$. For low values of ε and $\Delta x \gg \varepsilon$, the time scale of the hyperbolic part is much smaller than the time scale of the source term: the system is stiff. To avoid numerical difficulties, the exact solutions of (43) are therefore used to solve Step 2.

5.2. Numerical set-up

5.2.1. Shock tube problem

The RP problem of Section 2 is considered. The extended system of DNS with viscosity (vDNS$_e$) is compared with the hyperbolic system S_0. Discontinuous initial conditions for the vDNS$_e$ are:

$$\text{Shock tube}: \begin{cases} \rho|_{t=0} = \eta|_{t=0} = \begin{cases} \rho_L, & x < x_c \\ \rho_R, & x > x_c \end{cases}, \\ u|_{t=0} = w|_{t=0} = 0, \\ p|_{t=0} = \dfrac{\rho_R - \rho_L}{2}\delta(x - x_c). \end{cases} \tag{44}$$

The initial total energy of vDNS$_e$ is:

$$\mathcal{E}_e|_{t=0} = \frac{(\rho|_{t=0})^2}{2} + \frac{1}{4\,\rho|_{t=0}}\frac{(\varepsilon\, p|_{t=0})^2}{2}.$$

This energy is initially unbounded at $x = x_c$ because p does not belong to L^2. In practice, we consider $p = 0$ initially. This will yield a localised spurious solution. To circumvent this spurious solution, we also consider regularized initial data:

$$\text{Regularized Shock tube}: \begin{cases} \rho|_{t=0} = \eta|_{t=0} = \dfrac{\rho_L + \rho_R}{2} + \dfrac{\rho_R - \rho_L}{2}\tanh\left(\dfrac{x - x_c}{\zeta}\right), \\ u|_{t=0} = w|_{t=0} = 0, \\ p|_{t=0} = \dfrac{\rho_R - \rho_L}{2\zeta}\left(1 - \tanh\left(\dfrac{x - x_c}{\zeta}\right)^2\right). \end{cases} \tag{45}$$

The initial energy $\mathcal{E}_e|_{t=0}$ of the regularized problem is bounded. The spatial domain x is $[0; 500]$. The parameters are $\rho_L = 5$, $\rho_R = 1$, $x_c = 250$, CFL $= 0.9$, $\zeta = 0.1$. From Section 3.3, the viscosity function is $\mu = 2\rho\sqrt{\rho\,\mathcal{K}}$. The parameters of the extended Lagrangian (λ, β) are chosen in accordance with Section 4.5. The choice of the number of points N is done with respect to a wavelength $\ell^\star \leq \ell(0, \varepsilon)$, the latter being defined in Section 2.2. In practice, $\ell^\star \approx \ell(0, \varepsilon)/10$ is a good choice. Assuming 10 cells by wavelength, the number of cells is:

$$N = 100\,\frac{L}{\ell(0, \varepsilon)}.$$

In the proposed Riemann problem $L = 500$ and $\ell(0, \varepsilon) \approx 1$ which gives $N \approx 10^4$ cells.

5.2.2. Influence of the viscosity

Case $\tau = 0$. Figure 7 shows the numerical solution of the extended DNS when $\lambda = 500$, $\beta = 10^{-3}$ and $\varepsilon = 3$. The main features of the exact dispersive solution of S_ε, shown in Figure 2, are recovered: the dispersive shock lies inside the Whitham envelope, the plateau value ρ^* and the rarefaction wave are well captured.

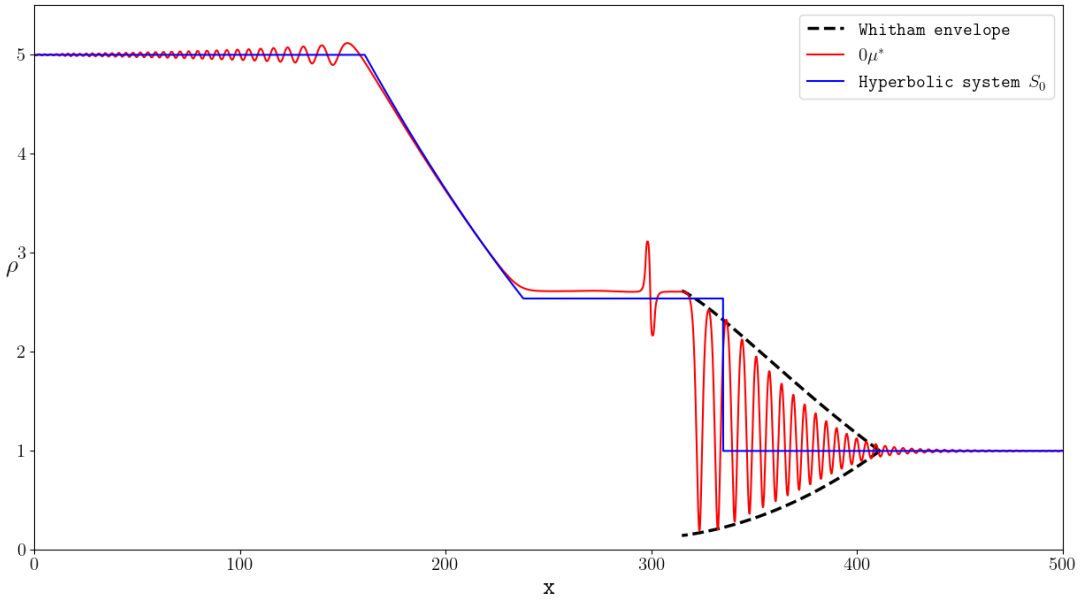

(a)

Figure 7: Shock tube problem: comparison between the exact solution of S_0 and the solution of vDNS$_e$ with $N = 2 \times 10^4$, $\lambda = 500$, $\beta = 10^{-3}$, $\varepsilon = 3$ and $\tau = 0$. A spurious oscillation induced by the initial discontinuity is observed near $x = 300$.

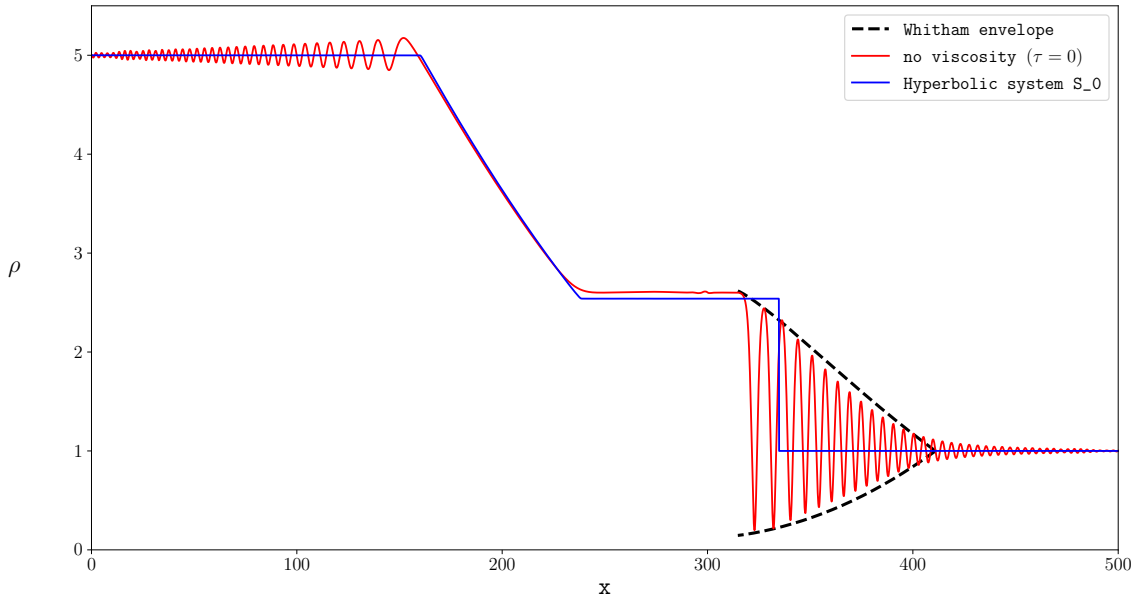

(a)

Figure 8: Regularized shock tube problem: comparison between the numerical solution of S_0 and the solution of vDNS$_e$ with $N = 2 \times 10^4$, $\lambda = 500$, $\beta = 10^{-3}$, $\varepsilon = 3$ and $\tau = 0$.

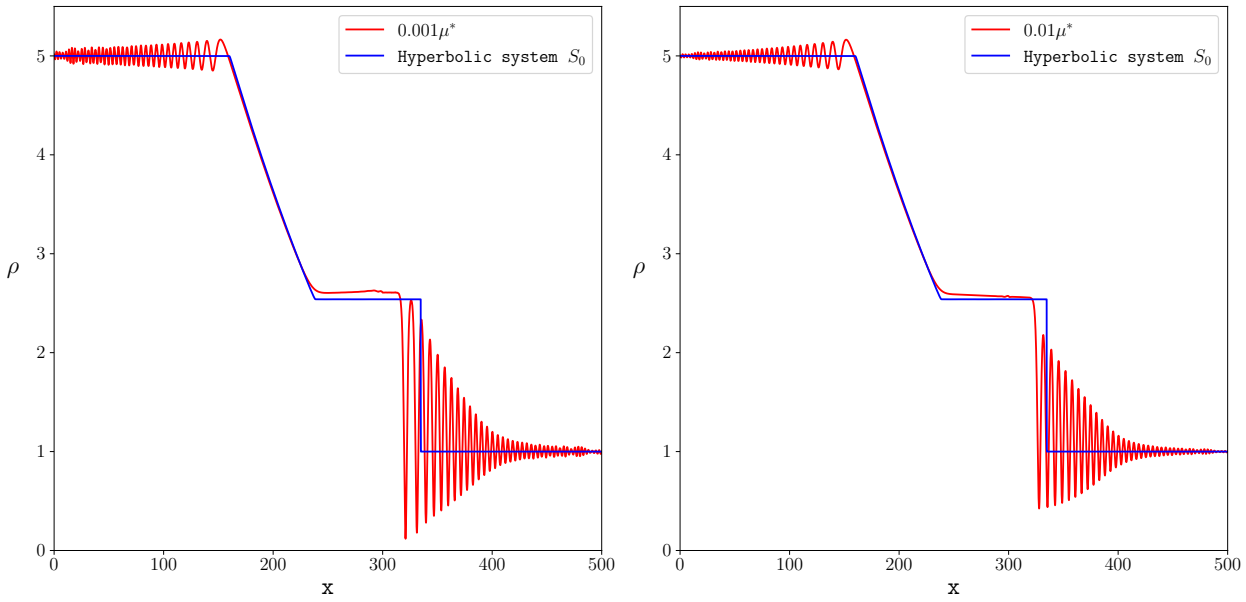

(a) $\tau = 0.001$

(b) $\tau = 0.01$

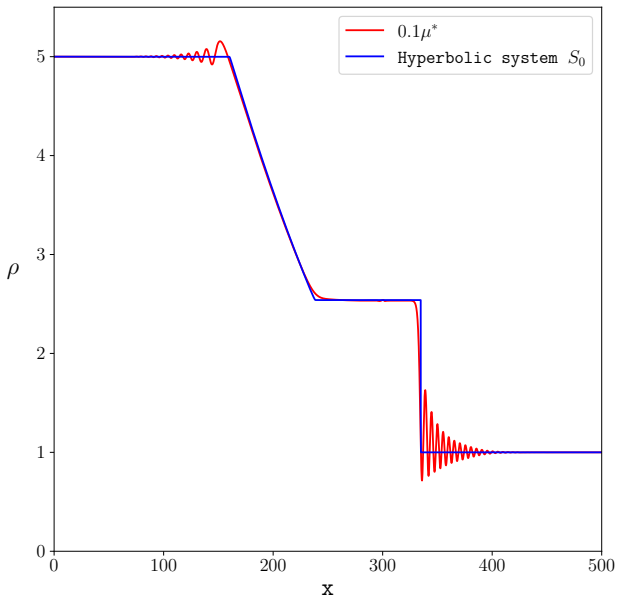

(c) $\tau = 0.1$

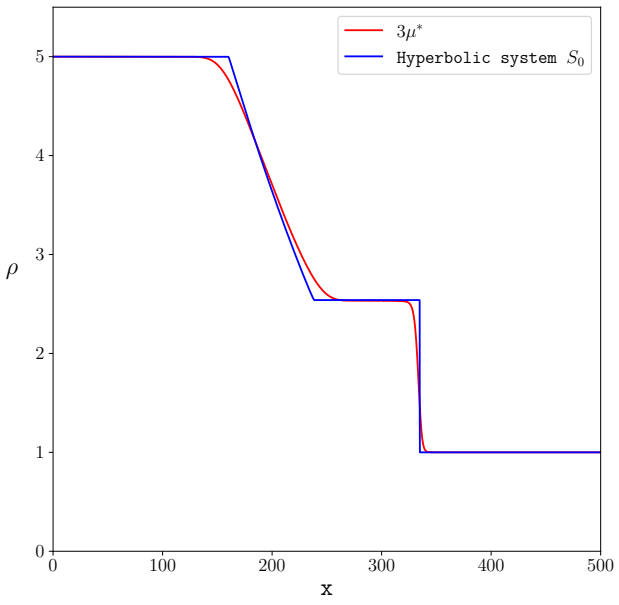

(d) $\tau = \hat{\tau} = 3$

Figure 9: Regularized shock tube problem. Effect of the viscosity on the solution of vDNS$_e$. $\tau \in \{0.001; 0.01; 0.1; 3\}$ with $N = 2^{15}$, $\varepsilon = 3$, $\lambda = 500$, $\beta = 0.001$.

Compared with Figure 2, additional features are observed. First, oscillations exist at the leading edge of the rarefaction wave. These oscillations decays when t increases [16]. Second, a spurious solution is localized at $x \approx 300$. It is induced by the discontinuous initial data (Section 5.2). Figure 8 shows the regularized version: the spurious solution is removed. In the following problems, we will always consider regularized initial data.

Case $\tau \neq 0$. Figure 9 illustrates the effect of the viscosity on the solution of vDNS$_e$ with the parameters of the previous case. For small viscosity, the amplitude of oscillations and the plateau value decrease. When the viscosity is even stronger that of the dispersion (d), that is when $\tau = \varepsilon$, the dispersive nature of the solution is removed. Indeed, the amplitude of the oscillations is null and the plateau value is close to the one of the hyperbolic system S_0. This result validates the analytical predictions of Section 3. The spurious solution is still present due to the dispersion parameter $\varepsilon \neq 0$.

Case $\tau = \varepsilon \to 0$. Figure 10 illustrates the evolution of the solution of vDNS$_e$ when $\varepsilon \to 0$, while keeping the equality $\tau = \varepsilon$ and respecting (33) for β. The viscous nature of the solution is removed when $\varepsilon \to 0$. The solution of the hyperbolic system is recovered in (c) and (d). The spurious solution has also disappeared. The only differences, around the edges of the rarefaction wave and around the shock, are due to the numerical dissipation of the scheme.

5.2.3. Double shock problem & double rarefaction problem

The regularized initial conditions for the vDNS$_e$ are:

$$\text{IC}: \begin{cases} \rho|_{t=0} = \eta|_{t=0} = 1, \quad u|_{t=0} = \dfrac{u_L + u_R}{2} + \dfrac{u_R - u_L}{2} \tanh\left(\dfrac{x - x_c}{\zeta}\right), \\ w|_{t=0} = -\dfrac{u_R - u_L}{2\zeta}\left(1 - \tanh\left(\dfrac{x - x_c}{\zeta}\right)^2\right), \quad p|_{t=0} = 0. \end{cases} \tag{46}$$

We set $u_L = 0$ for simplicity. When $u_R < 0$, two shock waves emerge from the center of the domain, whereas for $u_R > 0$, two rarefaction waves emerge. The parameters are $\zeta = 0.1$, CFL $= 0.9$. The results for both problem are compared to numerical solution of system S_0 in Figure 11 and Figure 12. Case (a) and (b) correspond to the dispersive case and the small dispersion and viscous limit, respectively. We emphasize the fact that, for both problems, the condition (33) has been extended to the case where $\bar{u} \neq 0$

$$\frac{\varepsilon^2}{4\beta\,\bar{\rho}^2} \geq (\bar{u} \pm \sqrt{\bar{\rho}})^2, \tag{47}$$

which yields the condition for β. The choice of $\pm$ is made to ensure the lowest value of β. On Figure 11 (a), the plateau value for the dispersive case is determined by the intersection of two Riemann invariant, as explained in section 2.2. Therefore, this plateau is greater than the plateau of the hyperbolic system. For the same reason, the plateau value in Figure 12 (a)

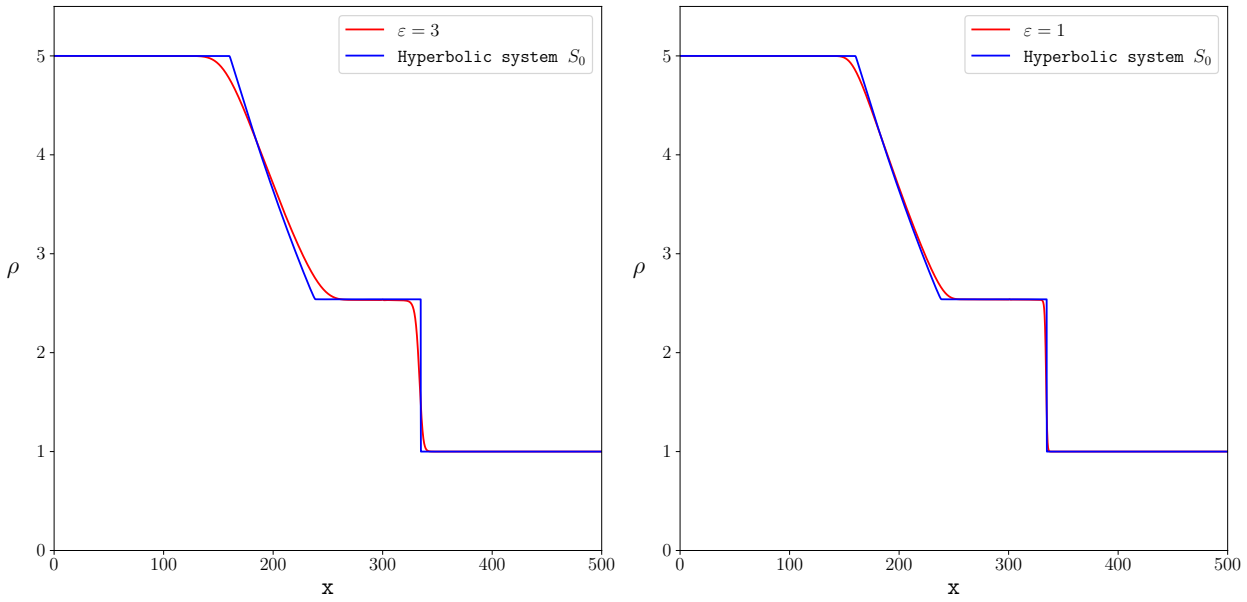

(a) $\tau = 3$, $\beta = 10^{-3}$ (b) $\tau = 1$, $\beta = 10^{-3}$

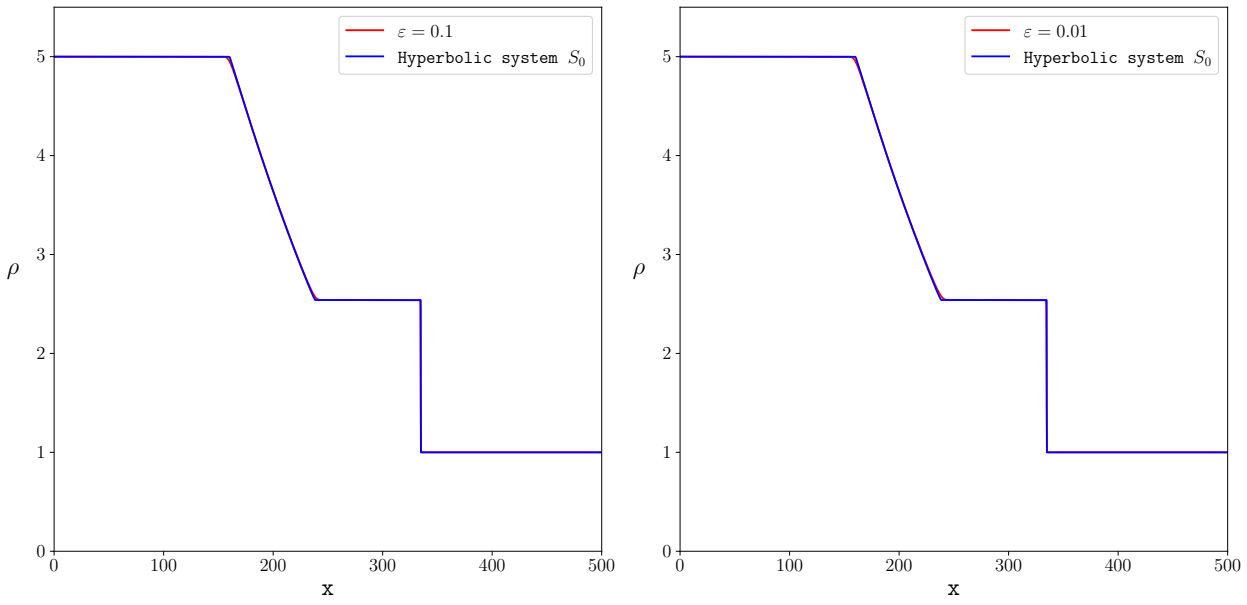

(c) $\tau = 0.1$, $\beta = 10^{-5}$ (d) $\tau = 0.01$, $\beta = 10^{-7}$

Figure 10: Regularized shock tube problem. Small dispersion limit and small viscosity limit of the solution of vDNS$_e$. $\tau = \varepsilon \to 0$ with $N = 2^{15}$, $\lambda = 500$ and variable β.

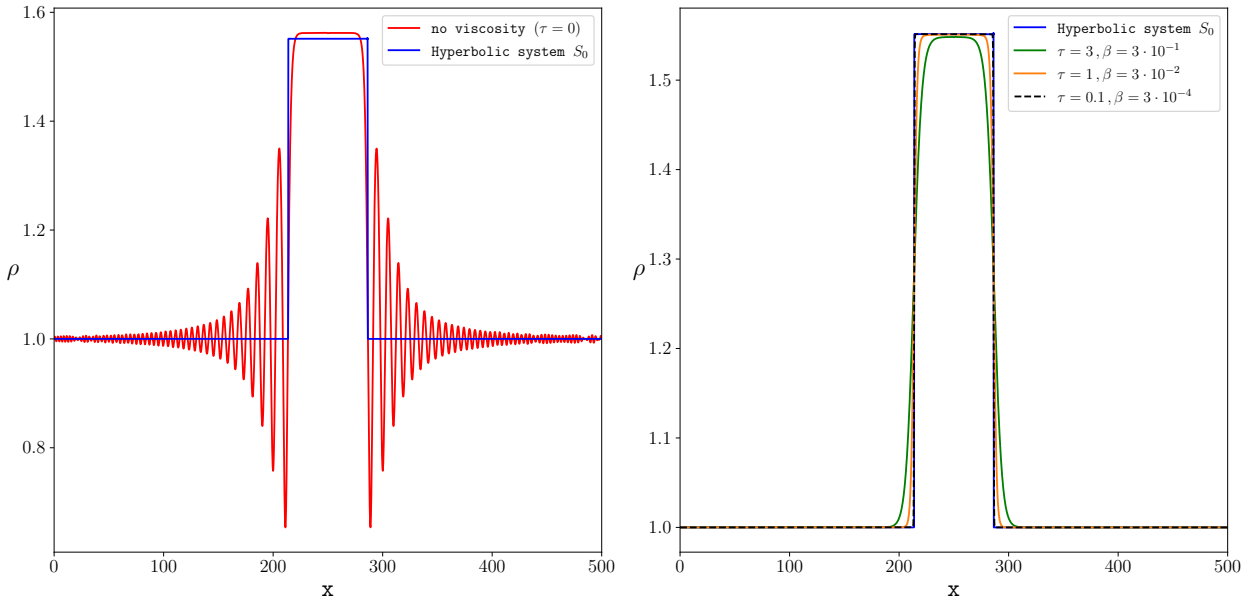

(a) $\tau = 0$, $\beta = 10^{-3}$, $\varepsilon = 3$ (b) $\tau = \varepsilon \to 0$

Figure 11: Double shock problem. Dispersive case in (a) and small dispersion and viscous limit on (b) of the solution of vDNS$_e$ with $N = 2^{15}$, $x_c = 270$, $\lambda = 500$ and variable β.

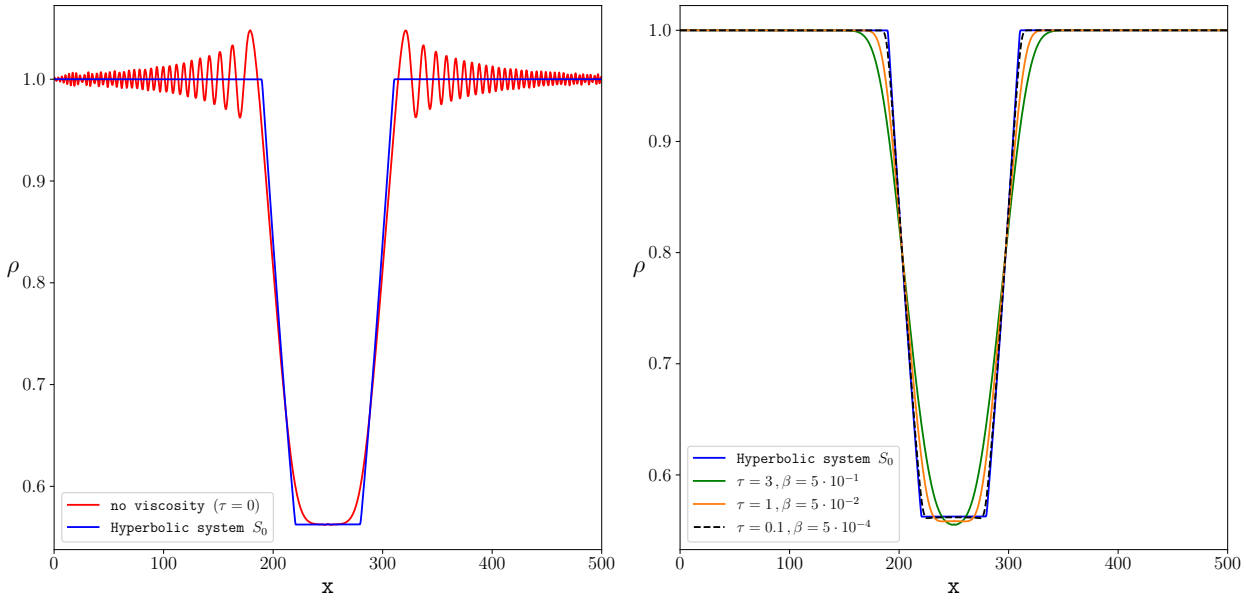

(a) $\tau = 0$, $\beta = 10^{-3}$, $\varepsilon = 3$ (b) $\tau = \varepsilon \to 0$

Figure 12: Double rarefaction problem. Dispersive case in (a) and small dispersion and viscous limit on (b) of the solution of vDNS$_e$ with $N = 2^{15}$, $x_c = 230$, $\lambda = 500$ and variable β.

are the same. Exact plateau values, for the different dispersive case, can be found in [36]. As shown in Figure 11 (b) and Figure 12 (b), the small dispersion and viscous limit yields solutions of the hyperbolic system.

6. Conclusion

This work was focused on a singular limit problem issued from Euler-Korteweg model. Based on the dispersion analysis and on the study of a travelling wave, an optimal viscosity $\mu(\rho)$ is introduced in the model. Doing so allows to recover the solutions of an Euler model in the limit of small dispersion and small viscosity. Numerical results, through the extended Lagrangian method, confirm the analysis. Classical shock waves and rarefaction waves are then recovered with vanishing dispersion.

The theoretical part of this work was essentially formal and based on : linear dispersion analysis, construction of travelling wave. More sophisticated mathematical tools are required to prove the convergence of NSK solution towards the solution of EK with vanishing dispersion and the optimal viscosity. Another mathematical analysis is required to prove the convergence of the extended Lagrangian method, in lines with [34]. Moreover, extension of the present approach to the two dimensional case, with convex equation of state, is appealing. Lastly, another extension of this work concerns the case of non-convex equation of state.

Acknowledgements. The authors are very grateful to Sergey Gavrilyuk for many advices and insights about nonlinear waves. This work was partially supported by ANR-ASTRID project SNIP ANR19ASTR001601.

[1] D. J. Korteweg, Sur la forme que prennent les équation de mouvement des fluides si l'on tient compte des forces capillaires causées par des variations de densité considérables mais continues et sur la théorie de la capillarité dans l'hypothèse d'une variation continue de la densité, Archives Néerlandaises des Sciences Exactes et Naturelles 6.

[2] J. D. V. der Waals, Théorie thermodynamique de la capillarité dans l'hypothèse d'une variation continue de densité, Archives Néerlandaises des Sciences Exactes et Naturelles 28.

[3] J. W. Cahn, J. E. Hilliard, Free energy of nonuniform system. I. Interfacial Free Energy, The Journal of Chemical Physics 28.

[4] V. Giovangigli, Kinetic derivation of diffuse-interface fluid models, Physical Review E 102.

[5] P. D. Lax, C. D. Levermore, The small dispersion limit of the Korteweg-deVries equation. I,II,III, Communications on Pure and Applied Mathematics 36 (3-5-6).

[6] M. A. Hoefer, M. J. Ablowitz, I. Coddington, E. A. Cornell, P. Engels, V. Schweikhard, On dispersive and classical shock waves in Bose-Einstein condensates and gas dynamics, Physical Review A 74.

[7] T. B. Benjamin, M. J. Lighthill, On cnoidal waves and bores, Proceedings of the Royal Society A 224 (1154) (1954) 448–460.

[8] R. S. Johnson, A non-linear equation incorporating damping and dispersion, Journal of Fluid Mechanics 42 (1) (1970) 49–60.

[9] J. L. Bona, M. E. Schonbek, Travelling-wave solutions to the korteweg-de vries-burgers equation, Proceedings of the Royal Society of Edinburgh Section A: Mathematics 101 (3-4) (1985) 207–226.

[10] H. Grad, P. N. Hu, Unified shock profile in a plasm, Physics of Fluids 10 (12) (1967) 2596–2602.

[11] A. V. Gurevich, L. P. Pitaevskii, Averaged description of waves in the korteweg-de vries-burgers equation, Journal of Experimental and Theoretical Physics 66 (3) (1987) 490–495.

[12] M. Affouf, R. E. Caflisch, A numerical study of riemann problem solutions and stability for a system of viscous conservation laws of mixed type, SIAM Journal on Applied Mathematics 51 (3) (1991) 605–634.

[13] P. Germain, P. G. LeFloch, The finite energy method for compressible fluids. the Navier-Stokes-Korteweg model, Communications on Pure and Applied Mathematics 69 (1) (2015) 3–61.

[14] C. Rohde, Fully Resolved Compressible Two-Phase Flow: Modelling, Analytical and Numerical Issues, in: New Trends and Results in Mathematical Description of Fluid Flows, Springer International Publishing, 2018, pp. 115–181.

[15] N. Favrie, S. Gavrilyuk, A rapid numerical method for solving SerreGreenNaghdi equations describing long free surface gravity waves, Nonlinearity 30 (7).

[16] F. Dhaouadi, N. Favrie, S. Gavrilyuk, Extended Lagrangian approach for the defocusing Non-Linear Schrodinger equation, Studies in Applied Mathematics, 142-3 (2019) 336–358.

[17] F. Dhaouadi, S. Gavrilyuk, J.-P. Vila, Hyperbolic relaxation models for thin films down an inclined plane, Applied Mathematics and Computation 433 (15).

[18] S. Bourgeois, N. Favrie, B. Lombard, Dynamics of a regularized and bistable Ericksen bar using an extended Lagrangian approach, International Journal of Solids and Structures 207 (2020) 55–69.

[19] S. Gavrilyuk, K. Shyue, Hyperbolic approximation of the BBM equation, Nonlinearity 35 (3) (2022) 1447–1467.

[20] S. Gavrilyuk, Multiphase Flow Modeling via Hamiltons Principle, in: F. dellIsola, S. Gavrilyuk (Eds.), Variational Models and Methods in Solid and Fluid Mechanics, Vol. 535 of CISM International Centre for Mechanical Sciences, Springer Vienna, 2014, Ch. 4, p. 163210.

[21] G. A. El, M. A. Hoefer, Dispersive shock waves and modulation theory, Physica D: Nonlinear Phenomena 333 (2016) 11–65.

[22] J. S. Rowlinson, B. Widom, Molecular Theory of Capillarity, Dover publications, INC., 1982.

[23] P. D. Lax, Hyperbolic Systems of Conservation Laws and the Mathematical Theory of Shock Waves, Society for Industrial and Applied Mathematics, 1973.

[24] E. Madelung, Quantentheorie in hydrodynamischer form, Zeitschrift fr Physik 40 (1927) 322326.

[25] A. V. Gurevich, A. L. Krylov, Dissipationless shock waves in media with positive dispersion, Journal of Experimental and Theoretical Physics 65 (5).

[26] R. J. LeVeque, Finite Volume Methods for Hyperbolic Problems, Cambridge Texts in Applied Mathematics, Cambridge University Press, 2002.

[27] E. F. Toro, Riemann Solvers and Numerical Methods for Fluid Dynamics, Springer, 1999.

[28] A. M. Kamchatnov, Gurevich-Piteavskii problem and its development, Uspekhi Fizicheskikh Nauk 191 (2021) 5287.

[29] G. B. Whitham, Linear and Nonlinear Waves, Pure & Applied Mathematics, Wiley-Interscience, 1999.

[30] P. D. Lax, Hyperbolic systems of conservation laws II, Communication on pure and applied mathematics 10 (1957) 537–556.

[31] E. Godlewski, P.-A. Raviart, Numerical Approximation of Hyperbolic Systems of Conservation Laws, Springer New York, NY, 1996.

[32] D. Serre, The structure of dissipative viscous system of conservation laws, Physica D: Nonlinear Phenomena 239 (15) (2010) 1381–1386.

[33] O. L. Métayer, S. Gavrilyuk, S. Hank, A numerical scheme for the GreenNaghdi model, Journal of Computational Physics 229 (6) (2009) 2034–2045.

[34] V. Duchêne, Rigorous justification of the Favrie-Gavrilyuk approximation to the Serre-Green-Naghdi model, Nonlinearity 32 (10) (2019) 3772–3797.

[35] R. Z. Sagdeev, C. F. Kennel, Collisionless shock waves, Scientific American (1991) 106–113.

[36] G. A. El, V. V. Geogjaev, A. V. Gurevich, A. L. Krylov, Decay of an initial discontinuity in the defocusing nls hydrodynamics, Physica D: Nonlinear Phenomena 87 (1) (1995) 186–192.

Appendix A. Lyapunov function: additional details

Equation (21) is multiplied by the integrating factor $-\frac{1}{\rho^2}\frac{d\rho}{d\xi}$ and integrated with respect to ξ. We obtain the following equation:

$$C_2 = \frac{1}{2}\frac{\mathcal{K}}{\rho}\left(\frac{d\rho}{d\xi}\right)^2 - e_h(\rho) - \frac{C_1}{\rho} + \frac{q^2}{2\rho^2} - \int_{\xi_0}^{\xi} \frac{\mu q}{\rho^4}\left(\frac{d\rho}{d\xi}\right)^2 d\xi. \tag{A.1}$$

We then define the Lyapunov function E:

$$E = \frac{1}{2}\frac{\mathcal{K}}{\rho}\left(\frac{d\rho}{d\xi}\right)^2 - e_h(\rho) - \frac{C_1}{\rho} + \frac{q^2}{2\rho^2} \tag{A.2}$$

such that we have the following property :

$$E - C_2 = \int_{\xi_0}^{\xi} \frac{\mu q}{\rho^4}\left(\frac{d\rho}{d\xi}\right)^2 d\xi \tag{A.3}$$

or equivalently

$$\frac{dE}{d\xi} = \frac{\mu q}{\rho^4}\left(\frac{d\rho}{d\xi}\right)^2 \tag{A.4}$$

Appendix B. Travelling wave: additional details

When $e_h = \rho/2$, the conditions (23) recover (5) and (6) for S_0 (Table 1): thus (23) amount to the Rankine-Hugoniot conditions. Therefore, we consider the RP problem (4) for which ρ_R and ρ_0 automatically verify (23) with D the shock wave's speed. The structure of the travelling wave is related to the structure of the extrema (e.g. stable foci). Those informations are obtained by solving an eigenvalue problem for the linearized version of the nonlinear ODE (21) and by looking at second derivatives of E:

$$\begin{aligned}
&\frac{\partial E}{\partial \frac{d\rho}{d\xi}} = \left(\frac{\mathcal{K}}{\rho}\right)\frac{d\rho}{d\xi}, \quad \frac{\partial^2 E}{\partial \frac{d\rho}{d\xi}^2} = \left(\frac{\mathcal{K}}{\rho}\right), \\
&\frac{\partial E}{\partial \rho} = \frac{1}{2}\left(\frac{\mathcal{K}}{\rho}\right)'\left(\frac{d\rho}{d\xi}\right)^2 + \frac{1}{\rho^2}\left(C_1 - \rho^2 e_h(\rho)' - \frac{q^2}{\rho}\right), \\
&\frac{\partial^2 E}{\partial \rho^2} = \frac{1}{2}\left(\frac{\mathcal{K}}{\rho}\right)''\left(\frac{d\rho}{d\xi}\right)^2 - \frac{2}{\rho^3}\left(C_1 - \rho^2 e_h(\rho)' - \frac{q^2}{\rho}\right) - \frac{1}{\rho^2}\left((\rho^2 e_h(\rho)')' - \frac{q^2}{\rho^2}\right)
\end{aligned}$$

Setting $c^2 = (\rho^2 e_h(\rho)')'$ and $M = \dfrac{(u-D)}{c} = \dfrac{q}{\rho c}$, this gives:

$$\frac{\partial^2 E}{\partial \rho^2} = \frac{1}{2}\left(\frac{\mathcal{K}}{\rho}\right)''\left(\frac{d\rho}{d\xi}\right)^2 - \frac{2}{\rho^3}\left(C_1 - \rho^2 e_h(\rho)' - \frac{q^2}{\rho}\right) - \frac{c^2}{\rho^2}\left(1 - M^2\right)$$

At the critical point ρ_c, $\left.\dfrac{\partial E}{\partial \rho}\right|_{\rho_c} = 0$ and $\left.\dfrac{d\rho}{d\xi}\right|_{\rho_c} = 0$ which equivalent to $C_1 = \rho^2 e_h(\rho)' + \dfrac{q^2}{\rho}$. Therefore, we have:

$$\left.\frac{\partial^2 E}{\partial \rho^2}\right|_{\rho_c} = \frac{{c_c}^2}{{\rho_c}^2}\left(M_c^2 - 1\right), \quad \frac{\partial^2 E}{\partial \frac{d\rho}{d\xi}^2} = \frac{\mathcal{K}}{\rho} > 0. \tag{B.1}$$

The thermodynamic pressure $\rho^2 {e_h}'$ is assumed to be a convex function of $1/\rho$. Therefore, c^2 is always positive. From (B.1), the state R corresponds to the supersonic region ($|M_R| > 1$) and E admits a local minimum at this state. The state 0 is the subsonic region ($|M_0| < 1$) and E admits a local maximum at this state. In the interval $I =]\rho_m; \rho_0[$, where ρ_m has to verify $E_0 = E(\rho_m, 0)$, E admits a unique minimum at $\rho_R \in I$ (Figure B.13-(a)). If $\rho \in I$ at $\xi = 0$

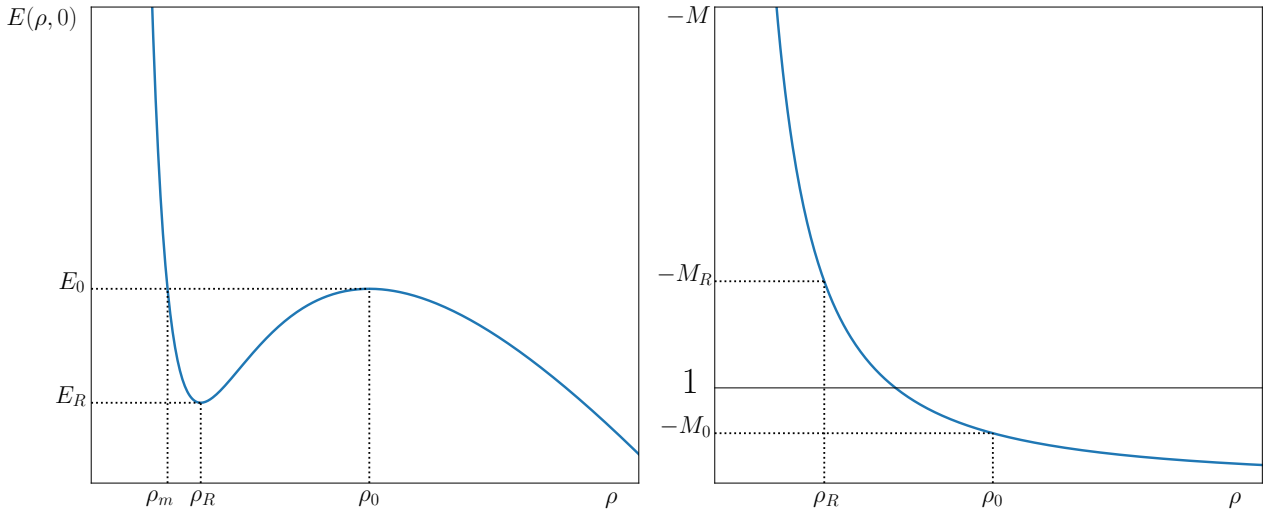

(a) $E(\rho, 0)$ (b) $-M(\rho)$

Figure B.13: Function $E(\rho, 0)$ and $-M(\rho)$, when $e(\rho) = \rho/2$, $\rho_R = 1$, $\rho_L = 5$.

and condition (22) is satisfied, the value $\rho(\xi)$ for any $\xi \neq 0$ remains in I. Therefore, $\rho(\xi) \to \rho_R$ when $\xi \to \infty$. The point ρ_R is asymptotically stable.

Appendix C. Matrix A and characteristic speeds

In (29), one has

$$\mathbf{A} = \begin{pmatrix} u & \rho & 0 & 0 & 0 \\ a & u & b & 0 & d \\ 0 & 0 & u & 0 & 0 \\ e & 0 & 0 & u & h \\ 0 & p & 0 & -1 & u \end{pmatrix}, \quad \mathbf{B} = \begin{pmatrix} 0 \\ 0 \\ w \\ \frac{\lambda}{\beta\rho}\left(1-\frac{\eta}{\rho}\right) - \tau\frac{\mu(\rho)}{\beta\rho^3}w \\ 0 \end{pmatrix}.$$

The coefficients are

$$a = 2{e_h}' + \rho {e_h}'' + \varepsilon^2 p^2 \left(\frac{\mathcal{K}'}{\rho} + \frac{1}{2}\mathcal{K}''\right) + \lambda\frac{\eta^2}{\rho^3}, \quad b = \frac{\lambda}{\rho}\left(1-\frac{2\eta}{\rho}\right), \quad e = -\frac{\varepsilon^2 p\mathcal{K}'}{\beta\rho},$$

$$h = -\frac{\varepsilon^2\mathcal{K}}{\rho\beta}, \quad d = \frac{p\,\varepsilon^2}{\rho}\left(\mathcal{K} + \rho\mathcal{K}'\right).$$

The characteristic equation is:

$$(u-\alpha)\left[(u-\alpha)^4 + (h - a\rho - pd)\,(u-\alpha)^2 + \rho(ed - ha)\right] = 0.$$

The characteristic speeds are:

$$\alpha^1 = u, \quad \alpha^{2,3} = u \pm c_1, \quad \alpha^{4,5} = u \pm c_2,$$

with

$$c_1 = \sqrt{\frac{1}{2}\left(c_e + \sqrt{(c_s)^2 + 4\frac{d^2}{\beta}}\right)},$$

$$c_2 = \sqrt{\frac{1}{2}\left(c_e - \sqrt{(c_s)^2 + 4\frac{d^2}{\beta}}\right)},$$

$$c_e = (\rho^2 {e_h}')' + \varepsilon^2 p^2\left(\frac{\mathcal{K}}{\rho} + 2\mathcal{K}' + \frac{1}{2}\rho\mathcal{K}''\right) + \frac{\varepsilon^2\mathcal{K}}{\rho\beta} + \lambda\left(\frac{\eta}{\rho}\right)^2,$$

$$c_s = (\rho^2 {e_h}')' + \varepsilon^2 p^2\left(\frac{\mathcal{K}}{\rho} + 2\mathcal{K}' + \frac{1}{2}\rho\mathcal{K}''\right) - \frac{\varepsilon^2\mathcal{K}}{\rho\beta} + \lambda\left(\frac{\eta}{\rho}\right)^2.$$

Appendix D. Exact solution for the relaxation step of the splitting

One can distinguish three regimes:

- Overdamped solution if $\left(\frac{\tau\mu^*}{\beta\rho^{*2}} > 2\sqrt{\frac{\lambda}{\beta}}\right)$:

$$r_{1,2} = \left(-\frac{\tau\mu^*}{2\beta\rho^{*3}} \pm \frac{1}{2}\sqrt{\left(\frac{\tau\mu^*}{\beta\rho^{*3}}\right)^2 - \frac{4\lambda}{\beta\rho^{*2}}}\right) \leq 0, \tag{D.1}$$

$$\eta(t) = \rho^* + (\eta^* - \rho^*)\frac{r_2 e^{r_1 t} - r_1 e^{r_2 t}}{r_2 - r_1} + w^* \frac{e^{r_2 t} - e^{r_1 t}}{r_2 - r_1}, \tag{D.2}$$

$$w(t) = (\eta^* - \rho^*)\frac{r_1 r_2 (e^{r_1 t} - e^{r_2 t})}{r_2 - r_1} + w^* \frac{r_2 e^{r_2 t} - r_1 e^{r_1 t}}{r_2 - r_1}. \tag{D.3}$$

- Critically damped solution if $\left(\frac{\tau\mu^*}{\beta\rho^{*2}} = 2\sqrt{\frac{\lambda}{\beta}}\right)$:

$$r_0 = -\frac{\tau\mu^*}{2\beta\rho^{*3}} \leq 0, \tag{D.4}$$

$$\eta(t) = \rho^* + (\eta^* - \rho^*)(1 - r_0 t)e^{r_0 t} + w^* t e^{r_0 t}, \tag{D.5}$$

$$w(t) = w^*(1 + r_0 t)e^{r_0 t} - r_0(\eta^* - \rho^*) r_0 t e^{r_0 t}. \tag{D.6}$$

- Underdamped solution if $\left(\frac{\tau\mu^*}{\beta\rho^{*2}} < 2\sqrt{\frac{\lambda}{\beta}}\right)$:

$$r_c = -\frac{\tau\mu^*}{2\beta\rho^{*3}} \leq 0, \quad \omega_c = \frac{1}{2}\sqrt{\frac{4\lambda}{\beta\rho^{*2}} - \left(\frac{\tau\mu^*}{\beta\rho^{*3}}\right)^2}, \tag{D.7}$$

$$\eta(t) = \rho^* + (\eta^* - \rho^*)\left(\cos(\omega_c t) - \frac{r_c}{\omega_c}\sin(\omega_c t)\right)e^{r_c t} + \frac{w^*}{\omega_c}\sin(\omega_c t)e^{r_c t}, \tag{D.8}$$

$$w(t) = -\omega_c(\eta^* - \rho^*)\left(1 + \left(\frac{r_c}{\omega_c}\right)^2\right)\sin(\omega_c t)e^{r_c t} + w^*\left(\cos(\omega_c t) + \frac{r_c}{\omega_c}\sin(\omega_c t)\right)e^{r_c t}. \tag{D.9}$$

Appendix E. Scaling of the fields with ε

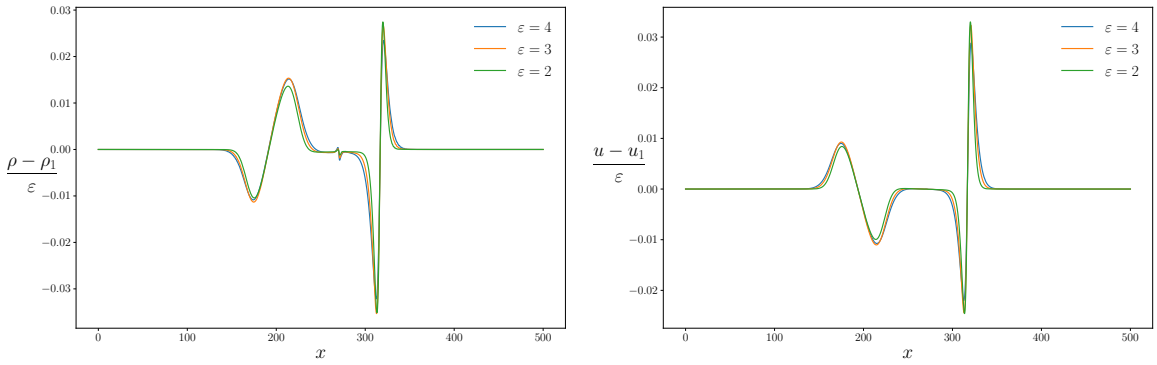

Figure E.14: Dependence of ρ and u on ε in the Riemann problem with $\rho_L = 2$, $\rho_R = 1$, $\lambda = 500$, $\beta = 10^{-3}$, $N = 2 \times 10^4$.

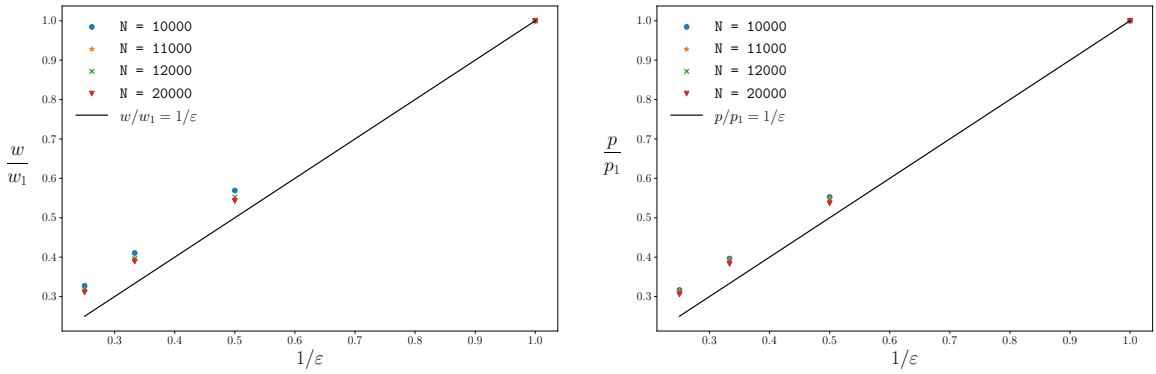

Figure E.15: Dependence of w and p on $1/\varepsilon$, for different number of cells N, in the Riemann problem with $\rho_L = 2$, $\rho_R = 1$, $\lambda = 500$, $\beta = 10^{-3}$

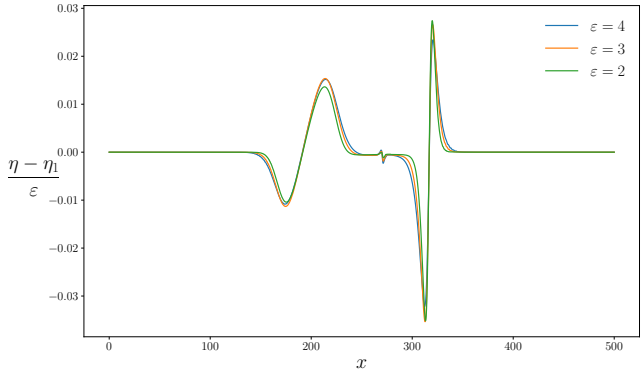

Figure E.16: Dependence of η on ε in the Riemann problem with $\rho_L = 2$, $\rho_R = 1$, $\lambda = 500$, $\beta = 10^{-3}$, $N = 2 \times 10^4$